



저작자표시-비영리-변경금지 2.0 대한민국

이용자는 아래의 조건을 따르는 경우에 한하여 자유롭게

- 이 저작물을 복제, 배포, 전송, 전시, 공연 및 방송할 수 있습니다.

다음과 같은 조건을 따라야 합니다:



저작자표시. 귀하는 원저작자를 표시하여야 합니다.



비영리. 귀하는 이 저작물을 영리 목적으로 이용할 수 없습니다.



변경금지. 귀하는 이 저작물을 개작, 변형 또는 가공할 수 없습니다.

- 귀하는, 이 저작물의 재이용이나 배포의 경우, 이 저작물에 적용된 이용허락조건을 명확하게 나타내어야 합니다.
- 저작권자로부터 별도의 허가를 받으면 이러한 조건들은 적용되지 않습니다.

저작권법에 따른 이용자의 권리는 위의 내용에 의하여 영향을 받지 않습니다.

이것은 [이용허락규약\(Legal Code\)](#)을 이해하기 쉽게 요약한 것입니다.

[Disclaimer](#)

Master's Thesis

**Numerical and Experimental Study on Vortex
Rope with MG V in the Micro-Class Hydro
Francis Turbine**

Supervisor Prof. Young-Ho LEE, Ph.D



February 2018

Department of Mechanical Engineering
Graduate School of Korea Maritime and Ocean University

Enkhtaivan Batmunkh

CONTENTS

ABSTRACT	VIII
ABBREVIATIONS.....	X
NOMENCLATURE	XII
CHAPTER 1. INTRODUCTION.....	1
1.1 Background.....	1
1.2 History of hydropower	2
1.3 Classification of the hydropower plant.....	3
1.3.1 River Power Plant (Run-Of-River).....	4
1.3.2 Pumped storage hydropower plant.....	5
1.3.3 Reservoir hydropower plant	5
1.3.4 Instream technology using existing facilities	6
1.4 Organization of hydropower plant.....	6
CHAPTER 2. HYDRO TURBINES	8
2.1 Classification of turbine.....	8
2.1.1 Based on head and quantity of water available	8
2.1.2 Classification based on action of the water flowing through runner	9
2.1.3 Classification based on Direction of flow of water in runner.....	10
2.1.4 Classification based on specific speed	10
2.2 Francis turbine	12
2.2.1 Components of the Francis turbine.....	12
2.2.2 Spiral Casing	13

2.2.3 Runner	13
2.2.4 Guide vanes and stay vanes	14
2.2.5 Draft tube.....	14
2.3 Cavitation in francis turbine	19
CHAPTER 3. PERFORMANCE AND DESIGN OPTIMIZATION	22
OF SETUP TURBINE	22
3.1 Modeling	22
3.2 Numerical analysis	28
3.2.1 Computational fluid dynamics (CFD).....	28
3.2.2 Grid discretization	29
3.2.3 Boundary condition.....	31
3.2.4 Hydraulic efficiency and power characteristic	32
3.2.5 Flow feature and pressure distribution	34
3.3 Unsteady flow analysis.....	41
3.3.1 Unsteady flow at full load	41
3.3.2 Unsteady flow at partial load.....	45
3.3.3 A draft tube swirl.....	46
3.3.4 Vortex rope in part flow	46
3.4 Signal analysis	52
3.5 Misaligned guide vane.....	55
CHAPTER 4. EXPERIMENTAL ANALYSIS.....	58
4.1 Experimental setup.....	58

4.2 Experimental apparatus specifications	60
4.2.1 Torque Transducer	60
4.2.2 Powder brake	62
4.2.3 Pressure transducers	63
4.2.4 Flow meter.....	64
4.3 Calibration and uncertainty analysis.....	66
4.4 Experimental procedure.....	67
4.4.1 Starting the Pump	67
4.4.2 Starting the Francis turbine	67
4.4.3 Hydraulic efficiency of experimental	67
4.5 PIV experiment.....	70
4.5.1 Overview of PIV Flow Visualization	70
4.5.2 Configuration of PIV experiment device.....	71
4.5.3 Lighting and tracking particles.....	73
4.5.4 Result of the PIV experiment	75
CHAPTER 5. CONCLUSION.....	82
ACKNOWLEDGEMENT	83
REFERENCES	84

List of Tables

Table 2.1 Classification of turbine based on head	8
Table 2.2 Cavitation factor values of specific speed	21
Table 3.1 Primary parameter	24
Table 3.2 Mechanical data	25
Table 3.3 Inlet dimensions of the turbine	26
Table 3.4 Outlet dimensions of the turbine	26
Table 3.5 Summary of mesh data	30
Table 3.6 Computational result at different flow rate	33
Table 4.1 Dimension of torque transducer	61
Table 4.2 Torque transducer specification	61
Table 4.3 Specification of Powder Brake	63
Table 4.4 Pressure transducer spec	64
Table 4.5 Flow meter specification.....	64
Table 4.6 Experimental results of the turbine	68

List of Figures

Figure 1.2 River power plant schema	4
Figure 1.3 Storage hydropower plant.....	5
Figure 1.4 Reservoir power plant	6
Figure 1.5 Typical arrangement of in stream technology hydropower projects	6
Figure 1.6 Arrangement of hydropower plant	7
Figure 2.1 Types of specific speed	11
Figure 2.2 Francis turbine	12
Figure 2.3 Energy loss in Francis turbine	14
Figure 2.4 Hydraulic principle of draft tube	16
Figure 2.5 Types of draft tube.....	17
Figure 2.6 Parameters of draft tube design	18
Figure 2.7 Types of cavitation	20
Figure 3.1 Velocity triangle	23
Figure 3.2 Turbine efficiency	26
Figure 3.3 Modeling of the fluid domain of the turbine for CFD simulation	27
Figure 3.4 Mesh dependence	29
Figure 3.5 3D unstructured grids generation by parts for the computational domain. .	30
Figure 3.6 Variation efficiency, discharge and head at different flow rate.....	34
Figure 3.8 Pressure distribution on the single blade suction and pressure side	36
Figure 3.9 Francis runner.....	37
Figure 3.10 Pressure coefficient of different single blades at different flow rates.	38
Figure 3.11 Velocity distribution in the spiral case at BEP	39
Figure 3.12 Velocity vector distribution in the spiral case at BEP	39

Figure 3.13 Pressure contour in the draft tube by different flow rate	40
Figure 3.14 Unsteady flow in the mid span of spiral casing	41
Figure 3.15 Velocity vector distribution at the spiral casing	42
Figure 3.16 Flow characteristics over the whole domain at full load	42
Figure 3.17 The average torque distribution at runner	43
Figure 3.18 Pressure distribution on the spiral	44
Figure 3.19 Torque distribution in the runner blade	44
Figure 3.20 Pressure distribution in the runner blade	45
Figure 3.21 Velocity streamline in the runner blade	45
Figure 3.22 Effect of turbulence model on shape of vortex rope	47
Figure 3.23 The vector field in the draft tube	48
Figure 3.25 Pressure region in mid-section of draft tube.....	50
Figure 3.27 Pressure recording locations	52
Figure 3.28 Amplitude spectra in runner blade	53
Figure 3. 29 Amplitude spectra in draft tube	54
Figure 3.30 MGV position.....	55
Figure 3.31 Variation efficiency, discharge and head at different guide vane angle	56
Figure 3.32 Influence of MGV on shape of vortex rope	57
Table 4.1 Dimension of torque transducer	61
Table 4.2 Torque transducer specification	61
Table 4.3 Specification of Powder Brake	63
Table 4.4 Pressure transducer spec	64
Table 4.5 Flow meter specification.....	64
Table 4.6 Experimental results of the turbine	68

Numerical and Experimental Study on Vortex Rope with MGV in Micro-Class Hydro Francis Turbine

Enkhtaivan Batmunkh

*Department of Mechanical Engineering
Graduate School of Korea Maritime and Ocean University*

ABSTRACT

Energy consumption is a huge part of our daily life. Today we gather most of our energy from coal, oil and natural gas also known fossil fuels. Generating electricity on our planet, requires plenty of massive power plants and transmission grid system delivery to the power. Renewable energy comes from a source that is not depleted when using such as wind, solar and hydropower. Hydropower is the largest source of renewable energy which is capture the energy of falling water to generate electricity as well can be efforts produce number of benefits such as a water supply, flood control and irrigation system. Micro-hydropower installation can provide power to the out-settlement or small community. These usually range between 5kW-100kW of electricity output.

In this study, numerical and experimental analysis of 3kW micro-class Francis turbine carried out to predict performance of the turbine. A Draft tube is one of the most important part of Francis turbine which connects the runner exit to the tailrace where the water is being finally discharged at atmospheric pressure from the reaction turbine. There are several issues in the draft tube like pressure pulsation, effect of cavitation on draft tube performance, vortex rope study etc. At part-load condition vortex form it hits structure constantly which is affect the performance of the turbine. This study focused on prediction

of vortex behavior at the draft tube and numerical results obtained the hydraulic performance of 3kW micro-class Francis turbine with the inlet pipe, a spiral casing with 12 guide vanes, 6 stay vanes and the runner having 13 blades and a draft tube. Ansys CFX software used to simulate for the numerical analysis of micro-class Francis turbine. Three misaligned guide vane (MGV) openings with 5 different MGV openings were chosen to analyze the influence of the pressure pulse in the turbine. Additionally, PIV technique was used to investigate flow velocity in the draft tube.

In the numerical simulation, different sets of operating points were selected to get performance characteristics of the turbine and best efficiency point indicated 91.67% efficiency at 0.02m³/s, power output 3.32kW. For misaligned guide vanes, more options can be tried out by misaligning more guide vanes, at higher angles. Additionally, based on the numerical analysis of a Francis turbine, the results for efficiency obtained from simulation are found to good agreement with the model results obtained from the manufacturer.

From the performed experiment on performance test of Francis turbine using the Francis turbine experimental set-up in the Flow Informatics Laboratory at Korean Maritime and Ocean University. The experimental analysis of the turbine showed a significant result. The turbine operated at different vane angle setting were obtained and tested by varying the parameters as a guide vane angle in the 6 different range of between 2-12 degrees, speed, and 500-1700 rpm respectively. The lowest difference between the experimental and numerical results was 2.03% and the maximum difference between the experimental and numerical results was 6.12 %. Numerical efficiency higher than experimental efficiency.

Key words: Francis turbine, Vortex rope, Misaligned guide vane, Computational Fluid Dynamic (CFD)

Abbreviations

CFD	Computational Fluid Dynamics
GGI	General Grid Interface
HPP	Hydropower Plant
KMOU	Korea Maritime and Ocean University
KW	Kilowatt
LE	Leading Edge
MGV	Misaligned Guide Vane
MH	Micro Hydro
PIV	Particle Image Velocimetry
PV	Photovoltaic
RNS	Reynolds Averaged Navier-Stokes
SST	Shear Stress Transport
TE	Trailing Edge

Greek symbols

α	Guide vane angle
β_1	Blade angle of runner inlet
β_2	Blade angle of runner outlet
η	Efficiency of the turbine
η_{cp}	Efficiency of draft tube
μ	Dynamic viscosity of fluid
ρ	Density of fluid
σ	Thoma's cavitation coefficient
σ_c	Cavitation factor values
v	Velocity
ω	Angular velocity
Ω	Speed number

Nomenclature

B_o	Blade width	[mm]
C_{m1}	Meridional velocity at the runner of inlet	[m/s]
C_{m2}	Meridional velocity at the runner of outlet	[m/s]
C_p	Pressure coefficient	-
C_{u1}	Swirl velocity at inlet of runner	[m/s]
C_{u2}	Swirl velocity at inlet of outlet	[m/s]
D_1	Diameter of runner inlet	[mm]
D_2	Diameter of runner outlet	[mm]
E	Specific energy	[J/Kg]
f_d	Dominating frequency	[Hz]
f_n	Rotational frequency	[Hz]
g	Acceleration due to gravity	[m/s ²]
H	Net head on the turbine	[m]
H_s	Suction head at the outlet of reaction turbine	[m]
H_v	Vapor head of water	[m]

h_f	The hydraulic losses in draft tube	[m]
k	Turbulence kinetic energy	[m ² /s ²]
N	Rotational speed of the turbine	rpm
N_{ED}	Dimensionless speed factor	[-]
N_s	Specific speed of the turbine	[-]
P_a	Shaft power	[kW]
P_t	Theoretical power	[kW]
T	Torque generated by runner	[Nm]
U_1	Peripheral velocity at inlet of runner	[m/s]
U_2	Peripheral velocity at runner of outlet	[m/s]
Q	Volumetric discharge	[m ³ /s]
Q_{ED}	Dimensionless speed	[-]

CHAPTER 1. INTRODUCTION

1.1 Background

Vortex rope becomes a critical issue when turbine operates under part load condition, especially for the Francis turbine. The rotation of the vortex rope is usually within 20-40% of the turbine speed, which causes severe rotating pressure fluctuations [1].

They are generated by unsteady vortex behavior as the incoming swirling flow decelerates in the diffuser cone, a hydrodynamic instability arises that looks like a rope swirling in the draft tube, the so-called vortex rope [2]. This phenomenon results in efficiency reduction. Due to the vortex rope high-pressure unsteady fluctuations on the walls of the draft tube, unwanted effects such as structural vibration and fatigue damage are likely to occur. Francis turbine experiences cyclic stresses, asymmetric forces on the runner, and wear and tear, all of which reduce the operating life of the components [2]. For the vortex problem, many researchers have explained on the formation of the vortex rope, vortex rope breakdown and furthermore mitigation of the vortex rope using control technique.

Computational fluid dynamics (CFD) is a very helpful technique which can predict the complex flow field in the hydraulic machines. It is used in different industries for different analytical capabilities. It's complicated to measure the vortex rope when the turbine works in actual operation. Therefore, it is possible to use CFD as a measurement tool for operating frequency, pressure pulsations and amplitudes which otherwise can be very difficult to determine in real life.. The primary goal of this study is to get accurate results from numerical analysis and experimental analysis. In particular, this work aims to understand the fundamental physical processes governing the formation of the vortex rope.

1.2 History of hydropower

Humans have been working with nature to perform work to achieve the better lifestyle for thousands of years. One of these approaches is by using water for power generation. In ancient, the Greeks and Romans have used water wheels for grinding wheat into flour which became basic of modern technology. It had a large surface /paddle/on the wheel and turn by water force when river flows is passing under the paddle but only some part of paddle wheel submerged underneath of water which means very lowest mechanical energy was obtained. This is a prototype for the reaction turbine which changes the direction of flow of a high-velocity fluid. Although the wheel was turned back and the hydraulic power was converted into mechanical energy, but it was very less amount of water strikes on the blades was converted useful work. Engineers realized that action of water would be able to more effective if water wheels cover by kind of assembly. In the mid-1700s German mathematician and naturalist, Johan Andres von Segner was built one of the earliest examples of reaction turbine. Working principle of his system same as an ancient water wheel but the water entered a cylindrical box containing the shaft or rotating wheel [3]. In 1920, Jean-Victor Poncelet developed an inward-flow turbine right away Benoit Fourneyron designed an outward-flow turbine.

In France, where there are more rivers, development on the water wheels carried out in first half of 19th century. At the time some of the key developments in hydropower technology represented by French engineer Benoît Fourneyron and former student of Burdin, who developed an outward-flow turbine that achieved close to 80% efficiency. Water was directed through the stationary inner core and then directed outward through curved horizontal guide vanes. The evolution of the modern hydropower, the first full-scale turbine designed by British –American engineer James Francis in 1849 was installed at the Boot Cotton Mills. Improvements of his design introduced water passed through the penstock to the turbine wheel and including curvature blade and fixed guide vane. One of the impressive advantages of his turbine design was the accuracy of performance prediction. Today, Hydropower become the leading renewable source for electricity generation globally, Reaching 1 064 GW of installed capacity in 2016, it represents about

71% of all renewable electricity and 16.4% of the world's electricity from all sources [4].

Fig 1.1 shows ancient water wheel.



Figure 1.1 Ancient water wheel

1.3 Classification of the hydropower plant

Hydraulic turbine is generally classified 2 main category which are reaction and impulse turbine. The main difference of those turbines are there is pressure change in fluid as fluid passes through runner of the reaction type turbine rather impulse type turbine where is no pressure change in the runner. According to the working principle hydropower plant can be classifiable different categorized. For example, it depends on by their capacity, type of construction, by their facility types and head etc [5].

Based on Capacity

- Large (More than 100MW)
- Medium (15-100MW)
- Small (Capacity is above the 1PMW)
- Mini (Capacity 300KW up to MW)
- Micro (Capacity 10kW up to 300KW)
- Pico (Capacity up to 10KW)

Based on Head

- High head (<300m)
- Medium Head (60m- up to 300m)
- Low head (>60m)

Based on facility types

- Run-off river hydropower plant
- Storage hydropower plant
- Pump storage water plant

Based on operation

- Manual hydropower plant
- Automatic plant

Based on type of load

- Base load hydropower plant
- Peak load hydropower plant

1.3.1 River Power Plant (Run-Of-River)

Usually, River power plant is small amount of water storage. It has generate electricity mainly from the available natural flow and elevation drop of the river showed in Fig 1.2. The pipeline is used to divert the water into the turbine, which is connected to the generator.



Figure 1.2 River power plant schema

1.3.2 Pumped storage hydropower plant

Storage hydro power plant is the one type of the hydropower plant which is uses the reservoir for the storage run-off. The working principle of the storage power plant storage most of the water energy is due to the potential energy of water in the reservoir. Its purpose is to store the water during excess flow periods and supplies during the same lean periods. The most of the storage hydropower plant is uses the dam to store the river in the reservoir. Figure 1.3 shows the storage hydropower plant.



Figure 1.3 Storage hydropower plant

1.3.3 Reservoir hydropower plant

In order to reduce the dependence on the variability of inflow, many hydropower plants comprise reservoirs where the generating stations are located at the dam toe or further downstream through tunnel or pipelines as per the electricity or downstream water demand as shown in Fig 1.4. Such reservoirs are often situated in river valleys. The high altitude lake makes up another kind of natural reservoirs. In these types of settings, the generating station is often connected to the lake serving as reservoir via tunnels coming up beneath the lake (lake tapping). For example, in Scandinavia natural high altitude lakes are the basic for high pressure systems where the heads may reach over 1000m. The design of the HPP and type of reservoir can built many dependent opportunities offered by the landscape [5].

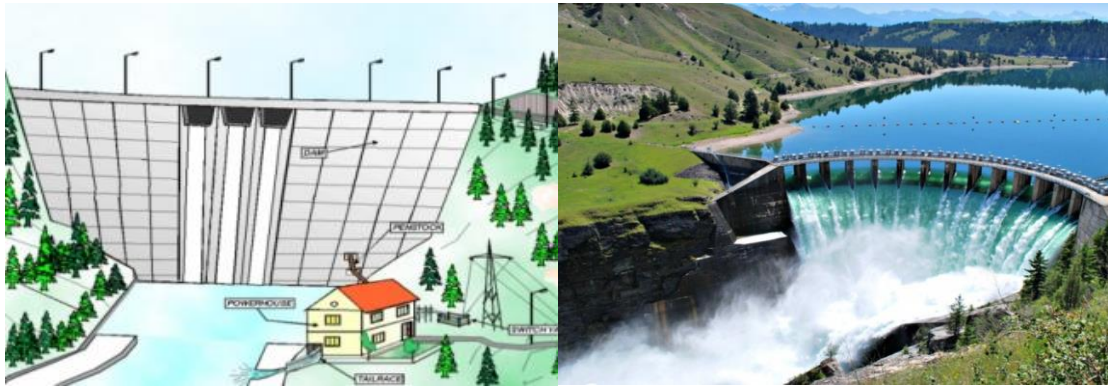


Figure 1.4 Reservoir power plant

1.3.4 Instream technology using existing facilities

To optimize existing facilities like weirs, barrages, canals or falls, small turbines can be installed for electricity generation. These are basically functioning like a run-of-river scheme as shown in Fig 1.5.

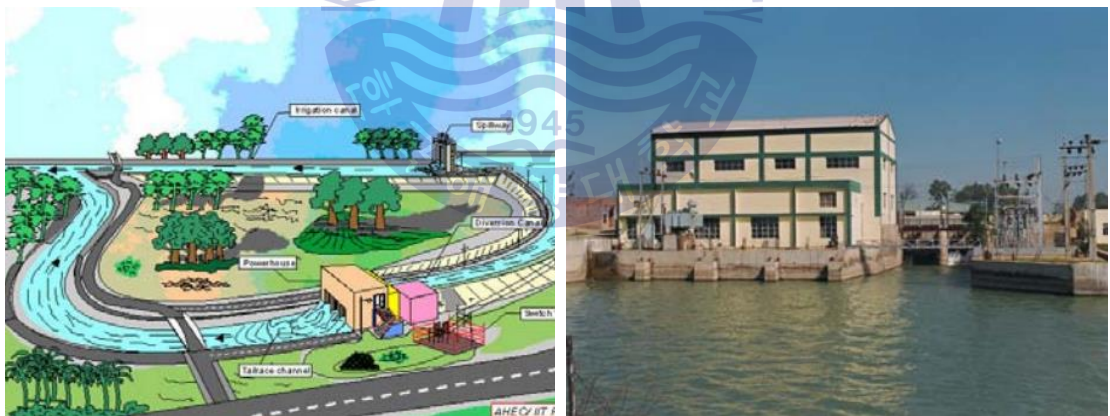


Figure 1.5 Typical arrangement of in stream technology hydropower projects

1.4 Organization of hydropower plant

The hydropower operating system requires three necessary things, running water, a turbine, and the generator. Generally, most of the method to produce electricity by hydropower is uses dams which is across the large rivers. The structures of the hydropower plant are given in the following section

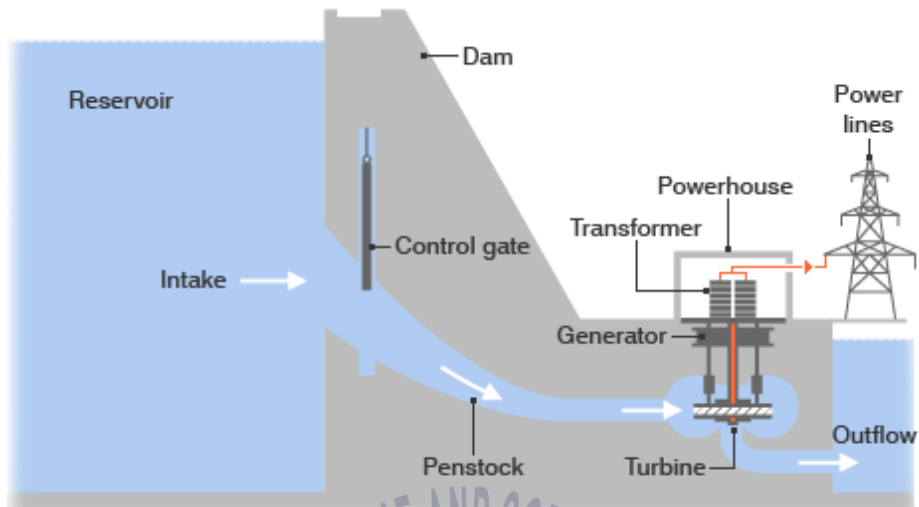


Figure 1.6 Arrangement of hydropower plant

The general principle of the hydropower plant is presented in Fig 1.6. The huge quantities discharge from reservoir in diverted by the intake and conduit to the turbine. A turbine starts to rotate due to the discharge hits on the turbine blade. The shaft in the generator is connected to the turbine. The electricity generated by shaft of the turbine rotates in the electric generator. Finally, the electricity passed through cable to the transformers are connected to the main national grid. This is the basic working principle of the hydro-electric power plant.

CHAPTER 2. HYDRO TURBINES

2.1 Classification of turbine

Hydro turbine is the heart of the hydropower plant which is convert mechanical energy to electrical energy.

The turbines are classified according to the following operating condition:

1. Head and quantity of water available
2. Hydraulic action of the water flowing through runner
3. Direction of flow of water in runner
4. The specific of the machines

2.1.1 Based on head and quantity of water available

According to head and quantity of water available, the turbines are categorized in Table 2.1.

Table 2.1 Classification of turbine based on head

Head classification	Turbine type		
	Impulse	Reaction	Gravity
High head (>50m)	Pelton Turgo		
Medium head (10-50m)	Crossflow Turgo Multi-jet Pelton	Francis	
Low (<10m)	Crossflow Undershot Waterwheel	Propeller Kaplan Francis	Overshot waterwheel Archimedes Screw

2.1.2 Classification based on action of the water flowing through runner

Based on action of the water flowing through runner, the hydraulic turbines can be classified into impulse and reaction turbine. In a turbine stage, the bleeding is of the impulse type and the pressure drop occurs only in the convergent nozzle guide vane passages. The steam of high-velocity gas were directed at the rotor blades, where the passages are constant in area and there is no further pressure drop. In a reaction turbine exactly the opposite takes place the entire pressure drop takes place between the rotor blades which have convergent passages the nozzle guide vanes do no more than guide the flow to the rotors. The turbine is driven by the reaction force resulting from the accelerating gas through the convergent blade passages [7].

Impulse turbine

The impulse turbine generally uses the velocity of the water to move the runner and discharges to atmospheric pressure. The water stream hits each bucket on the runner and there is no suction on the downside of the turbine, and the water flows out the bottom of the turbine housing after hitting the runner. An impulse turbine is generally suitable for high head and low flow applications [6]. The nozzle is a passage for the flow of steam where the pressure is converted into kinetic energy. its main function is to produce a jet of steam with high velocity the steam from the boiler at high pressure enters the converging part of the nozzle as it passes through the and divergent portion of the nozzle. It gains very high velocity and the nozzle helps to convert the potential energy of the steam into kinetic energy when it expands through the nozzle. The increased velocity is utilized for rotating the turbine blades mounted on the shaft. When the velocity increases the pressure decreases. The wheel on the rotor is fitted over a shaft from which the useful power is available. It is a rotary element of the turbine on which moving blades are fixed. The rotor consists of circular disk fixed to a horizontal shaft. The rotor shaft is mounted on suitable bearings. Blades on the periphery of the rotor a large number of blades are fixed. The steam jet from the nozzle impinges on the surface of the glares due to which the rotor

rotates. The surface of the blades is made smooth to frictional losses casing. The casing is the outside steam tight steel cover of the steam turbine which encloses the rotor blades etc.

Reaction turbine

Reaction turbine represents by Newton's third law of motion (For every action, there is an equal and opposite reaction). Only a portion of fluid energy is converted into kinetic energy before the fluid enters the turbine runner. This work is chiefly done by the change in pressure head and partly by the change in pressure head.

2.1.3 Classification based on Direction of flow of water in runner

When the water is flowing through the runner and it moves to the part of the machine. Based on flow through the turbine, the hydraulic machines are classified into

1. Tangential flow (Pelton turbine)
2. Radial flow (Francis turbine)
3. Axial flow (Kaplan turbine, propeller turbine)
4. Mixed flow (Modern Francis turbine)

2.1.4 Classification based on specific speed

Specific speed defined as the speed of a turbine which is identical in shape, geometrical dimensions, blade angles and gate opening etcetera with the actual turbine, but such size will develop the unit power when working under head. Figure 2.1 shows the range of specific speed.

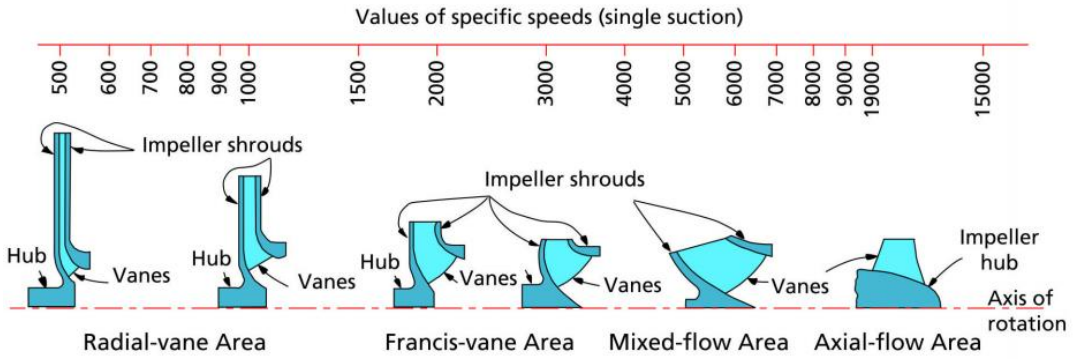


Figure 2.1 Types of specific speed



2.2 Francis turbine

Francis turbine is a mixed flow turbine. The main characteristics of the Francis turbine is it can operate from lower head till medium head. In 1849, James Bicheno Francis introduced the new turbine after major improvements on the design which is installed at the Boot Cotton Mills. Today, most of the hydropower plants installed Francis turbine on their application, which is operating in medium head and reaction kind of turbine. Francis turbine contains casing, runner, guide vane, stay vane and draft tube. Casing is covering of the turbine which prevents a turbine from any mechanical damage. The runner is the heart of the turbine and also rotational part of the turbine. In the runner, water will come in the radial direction and will go passes axil direction. Guide vanes are the stationary part of the turbine which keeps the water for rotating in the runner. A draft tube is a final part of the Francis turbine and the pressure and kinetic energy both are used in the Francis turbine for rotating the runner. Figure 2.2 shows components of the Francis turbine

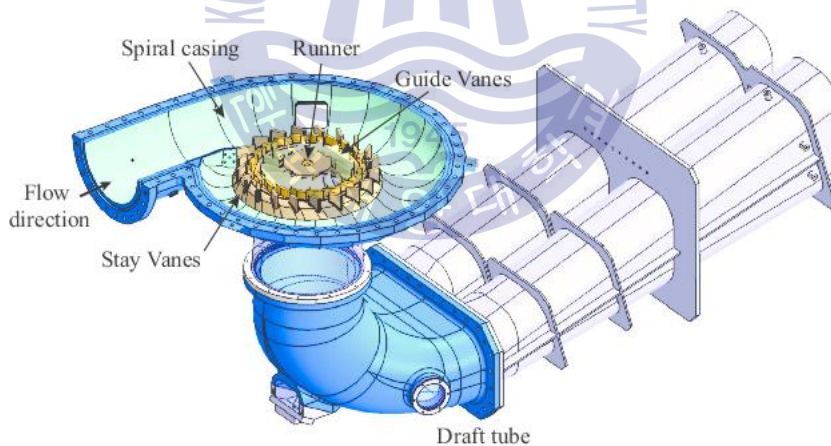


Figure 2.2 Francis turbine

2.2.1 Components of the Francis turbine

Francis turbine consists of the main following parts, as spiral casing, stay vane, guide vane, runner and draft tube [6].

2.2.2 Spiral Casing

Spiral case is the first component of the Francis turbine which distribute the water equally to the guide vane cascade.

2.2.3 Runner

The runner is the heart of the turbine. The runner has series of curved vanes which is located between hub and band in the angular space. When water hits blades of the runner force is develop of the blades due to that torque will be develop by the runner. The shape of the blades of a Francis runner is complex. The exact shape depends on its specific speed. It is obvious from the equation of specific speed that higher specific speed means lower head. This requires that the runner should admit a comparatively large quantity of water for a given power output and at the same time the velocity of discharge at runner outlet should be small to avoid cavitation. In a purely radial flow runner, as developed by James B. Francis, the bulk flow is in the radial direction. To be more clear, the flow is tangential and radial at the inlet but is entirely radial with a negligible tangential component at the outlet. The flow, under the situation, has to make a 90o turn after passing through the rotor for its inlet to the draft tube. Since the flow area (area perpendicular to the radial direction) is small, there is a limit to the capacity of this type of runner in keeping a low exit velocity. This leads to the design of a mixed flow runner where water is turned from a radial to an axial direction in the rotor itself. At the outlet of this type of runner, the flow is mostly axial with negligible radial and tangential components. Because of a large discharge area (area perpendicular to the axial direction), this type of runner can pass a large amount of water with a low exit velocity from the runner. The blades for a reaction turbine are always so shaped that the tangential or whirling component of velocity at the outlet becomes zero ($V_{w_2} = 0$). This is made to keep the kinetic energy at the outlet a minimum.

2.2.4 Guide vanes and stay vanes

The primary purpose of the guide vane is to convert the pressure energy of the fluid into the kinetic energy and to alter the direction of the flow at design angles to the runner blades. It will guide the water to pass to the runner blades. Moreover, the guide vanes are pivoted and can be turned by a suitable governing mechanism to regulate at flow while the load changes.

2.2.5 Draft tube

In the first half of the nineteenth century, the draft tube had been used to connect reaction turbine [8]. A draft tube is significantly affected in reaction turbine efficiency. Generally, low head turbines are going to be of the reaction type turbine [10]. Low heads and high flow rates can be the main reason for loss of efficiency in draft tube as shown in Fig 2.3. The main purpose of the draft tube is to reduce the velocity of the discharged water to minimize the loss of kinetic energy at the outlet [9].

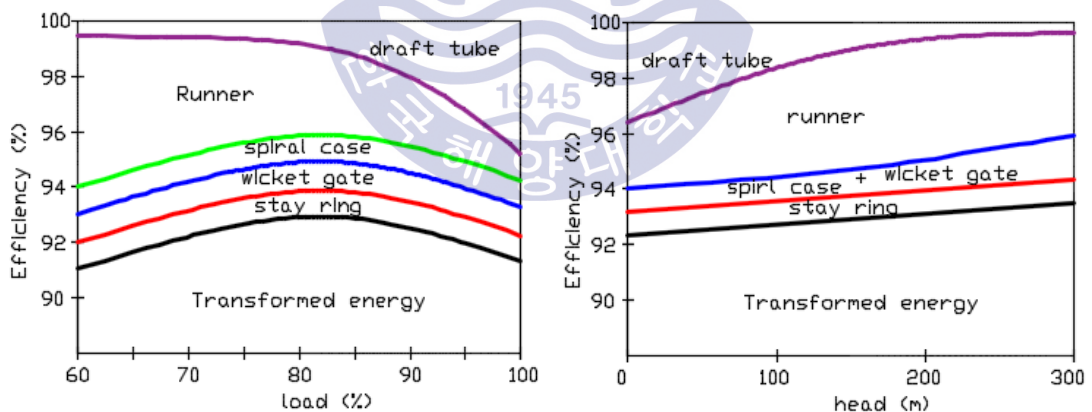


Figure 2.3 Energy loss in Francis turbine

Principles of operation of a draft tube

The principle of a draft tube can be outlined by applying Bernoulli's equation to inlet (1-1) and outlet (2-2) of draft tube as shown in Fig 2.4. Bernoulli's equation as given in equation (2.1)

$$\frac{p_1}{\rho g} + z_1 + \frac{\alpha_1 V_1^2}{2g} = \frac{p_2}{\rho g} + z_2 + \frac{\alpha_2 V_2^2}{2g} + h_f \quad (2.1)$$

Where:

- p – Absolute pressure
- z_1 – Height
- α – Kinetic energy correction factor
- V – Main velocity
- h_f – Hydraulic losses in draft tube

The absolute pressure p at section 2-2 can furthermore be expressed as $p_2/\rho g = z_2 + p_{atm}/\rho g$ where p_{atm} is the atmospheric pressure. An assuming that the turbine installation height H_s is approximately equal to z_1 , equation (2.2) reduces to

$$\frac{p_1}{\rho g} = \frac{P_{atm}}{2g} = \left\{ H_s + \left(\frac{\alpha_1 V_1^2}{2g} + \frac{\alpha_2 V_2^2}{2g} - h_f \right) \right\} \quad (2.2)$$

An interpretation of equation (2.2) is that the draft tube generates a low pressure region underneath the runner, which can be utilized by the turbine. This lower pressure, consist of two terms; static fall of pressure and dynamic fall of pressure, H_s and $\alpha_1 V_1^2/2g - \alpha_2 V_2^2 - h_f$

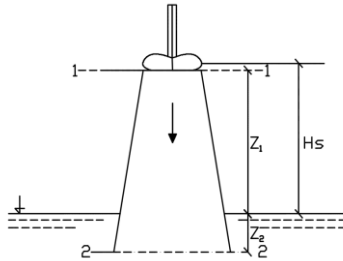


Figure 2.4 Hydraulic principle of draft tube

The performance of a draft tube (or a diffuser) is generally described by four performance metrics. These are the actual pressure recovery C_p , the ideal pressure recovery C_{pi} , the draft tube efficiency η_{cp} and the loss factor ζ . These are described in equations (2.3) to (2.6).

$$C_p = \frac{p_1 - p_2}{\rho(\alpha_1 V_1^2)/2} \quad (2.3)$$

$$C_{pi} = 1 - \frac{\alpha_2 \left(\frac{V_2}{V_1}\right)^2}{\alpha_1} = 1 - \frac{\alpha_2 \left(\frac{A_1}{A_2}\right)^2}{\alpha_1}, \quad (2.4)$$

$$\eta_{cp} = \frac{C_p}{C_{pi}}, \quad (2.5)$$

$$\zeta = C_{pi} - C_p = 1 - C_p - \frac{\alpha_2 \left(\frac{A_1}{A_2}\right)^2}{\alpha_1}, \quad (2.6)$$

Where, A – is the cross – section area

Types of draft tube

The draft tube is an integral part of reaction turbine, and its design criteria should be specified by the turbine manufacturer. There are following types of draft tube used in hydropower plant as shown in Fig 2.5. Those are depending on the power output and orientation of the axis rotation.

1. The straight conical draft tube
2. Elbow type draft tube

3. The bell mouth spreading draft tube

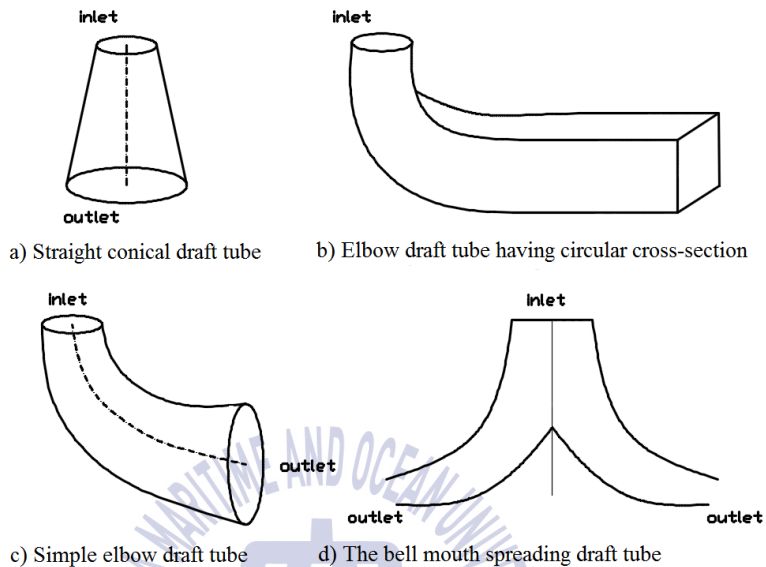


Figure 2.5 Types of draft tube

The straight conical draft tube is commonly used for Francis turbine. It has excellent hydraulic characteristics and efficiency of the conical draft tube is around 85% up to 90%. The straight conical draft tube can be used to small and medium-sized runner diameter does not exceed more than 2 meter. Usually length of draft tube is around 2 to $2.5D_1$

Curved (elbow) draft tubes are used when turbine has to be placed close to the tail-race, therefore, it is basic type in vertical hydraulic turbines of medium and large capacities. It helps to cut down the cost of excavation and their exit diameter should be as large as possible to recover kinetic energy at the outlet of the runner. The elbow types of draft tubes are approximately reached 60% efficient. The shape and dimensions of a curved draft tube depends on the turbine type and size. For example, exist there draft tubes with sharp heels, piers, guides and inside cones [7]. In general, the elbow draft tubes are consist of three parts namely cone, elbow and diffuser. The initial part of the tube is similar to the straight conical draft tube.

The bell mouth spreading draft tube is a straight axis tube but differs from the conical draft tube in the shape of its wall, which are shaped on the basis of some-liner law. The shape of resembles a trumpet with sharp flare at the exit [7].

Design of draft tube

Geometric parameterization

The draft tube design is based on the following dimensions of the book “Draft tubes of Hydro Electric Stations” by Gubin MF 1973 [8]. Geometric parameterization of the draft tube illustrated in Fig 2.6

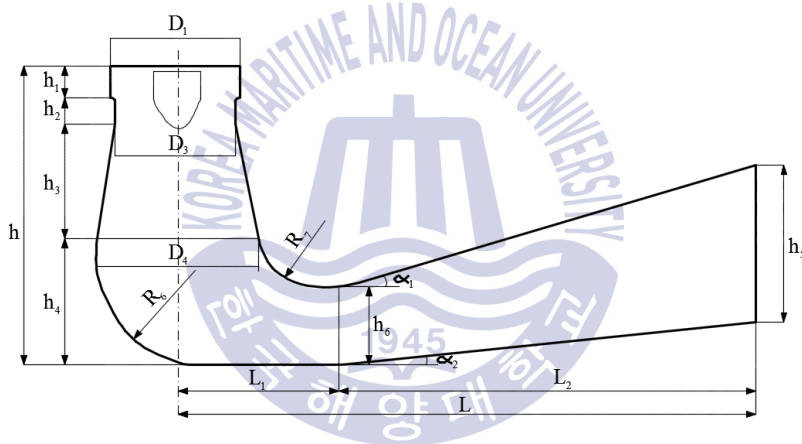


Figure 2.6 Parameters of draft tube design

2.3 Cavitation in Francis turbine

Cavitation is one of the difficulties in hydro machinery. Design, operation and refurbishment of hydraulic turbines, pumps or pump-turbine are strongly related to cavitation flow phenomena, which may occur in either the rotating runner-impeller or the stationary parts of the machine. Cavitation in Francis turbine may occur at the outlet of runner and at the inlet of the draft tube where are pressure drops below the vapor pressure. The following different forms cavitation occur in Francis turbine.

1. Leading edge cavitation
2. Travelling bubble cavitation
3. Draft tube swirl
4. Inter-blade vortex cavitation

Thoma cavitation factor (σ) is a dimensionless number suggested by Prof. D. Thoma which can be used to determine the region where the cavitation process occurs. [9]. Mathematically it is written as equation (2.7)

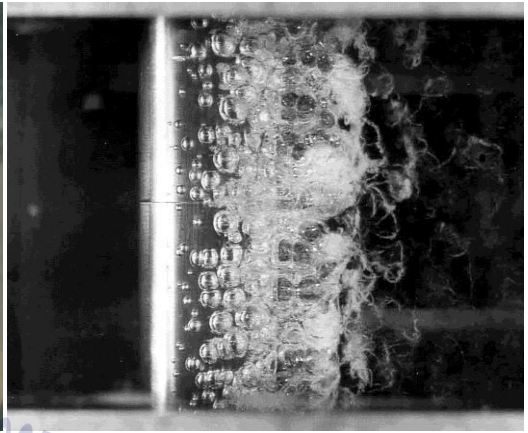
$$\sigma = \frac{H_b - H_s}{H} = \frac{(H_{atm} - H_v) - H_s}{H} \quad (2.7)$$

Where,

H_b	Barometric pressure head of water	[m]
H_{atm}	Atmospheric pressure head of water	[m]
H_s	Suction pressure at the outlet of reaction turbine / or height of turbine runner above the water tail race	[m]
H_v	Vapor pressure of water	[m]
H	Net head on the turbine	[m]



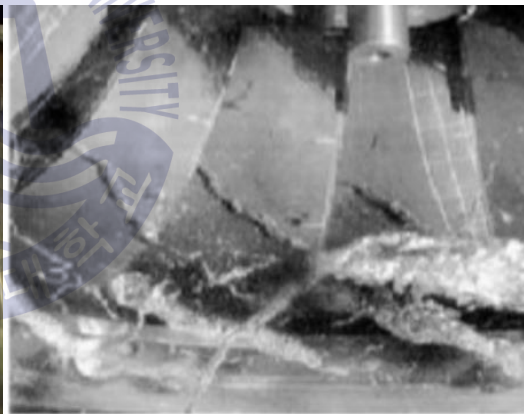
a) Leading edge cavitation



b) Traveling bubble cavitation



c) Draft tube swirl



d) Inter blade vortex

Figure 2.7 Types of cavitation

Cavitation can be avoided in the turbines, If and only If $\sigma > \sigma_c$.

For Francis turbine:

$$\sigma_c = 0.625 \times \left(\frac{N_s}{380.78} \right)^2 \quad (2.8)$$

Values of σ_c for different values of specific speed as shown in Table 2.2.

Table 2.2 Cavitation factor values of specific speed

Specific speed	89	178	267	355	444
σ_c	0.025	0.23	0.40	0.40	0.64



CHAPTER 3. PERFORMANCE AND DESIGN OPTIMIZATION OF SETUP TURBINE

3.1 Modeling

The head and flow rate are the main criteria that are used as preliminary parameters for the design of Francis runner. These two parameters are given as $H=20\text{m}$ and $Q=0.02\text{m}^3/\text{s}$. From this, theoretical power could be computed and expressed as

$$P_t = \rho g Q H \quad (3.1)$$

Considering 70% efficiency of the turbine

$$P_r = \rho g Q H \quad (3.2)$$

When turbine rotational speed given $n=1800\text{rpm}$, Turbine specific speed expressed

$$N_s = \frac{n\sqrt{P}}{H^{5/4}} \quad (3.3)$$

Before choose the diameter at the outlet we assume empirical relation for the outlet angle of the runner blade $13 < \beta_2 < 22^\circ$ (lowest value for highest head). $35 < u_2 < 43\text{m/s}$. Diameter at the outlet expressed as

$$D_2 = \sqrt[3]{\frac{240 \times Q}{\pi^2 \times n \times \tan \beta_2}} \quad (3.4)$$

The peripheral velocity of the turbine expressed as,

$$u_2 = \frac{\pi \times n \times D_2}{60} \quad (3.5)$$

The meridional velocity at the runner expressed as,

$$C_{m2} = \frac{4 \times Q}{\pi \times D_2^2} \quad (3.6)$$

Dimensions of the inlet, Hydraulic efficiency of the turbine expressed by

$$\eta_h = \frac{(U_1 C_{u1} - U_2 C_{u2})}{g H_h} = 2(u_1 c_{u1} - u_2 c_{u2}) \quad (3.7)$$

Where, U is the peripheral velocity of the runner blades C_u is the components of absolute velocity in the direction of the U . at the best efficiency point, $c_{u2} = 0$. Design is the done no whirl condition expressed as,

$$\eta_h = 2(u_1 c_{u1}) \quad (3.8)$$

Using the empirical relation to compute the reduced peripheral velocity of the blade at inlet expressed as,

$$0.7 < u_1 < 0.8 \quad (3.9)$$

Now, the diameter of the runner inlet is,

$$D_1 = \frac{u_1 \times 60}{n \times \pi} \quad (3.10)$$

Height of the inlet expressed as,

$$c_{m2} = 1.1 \times c_{m1} \quad (3.11)$$

$$B_1 \times D_1 \times \pi = \frac{1.1 \times \pi \times D_2^2}{4} \quad (3.12)$$

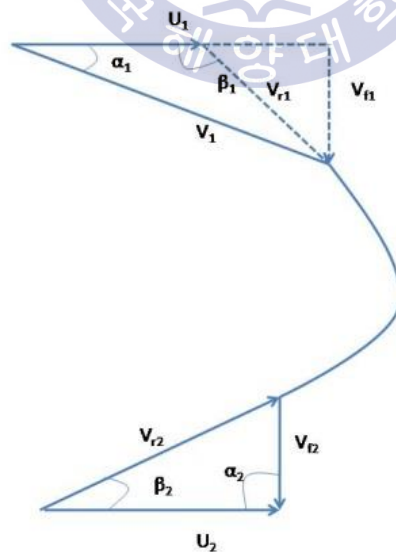


Figure 3.1 Velocity triangle

A 3kW micro-class Francis turbine designed and manufactured by “Shinhan Precision” Co.,Ltd. Table 3.1 and Table 3.2 show the turbine parameters. The design equation solver was prepared in MS Excel v.2013 to calculate the above equations and generate the design dimensions of the runner and guide vanes along with the corresponding velocity diagrams at inlet and outlet as well turbine mechanical data calculated in HPP Design online calculation software as shown in Fig 3.2.

Table 3.1 Primary parameter

Net head	20	m
Max discharge	0.02	m ³ /s
Rotational speed	1800	rpm
Turbine power	2.74	kW



Table 3.2 Mechanical data

i Hydro Power Plants sizing details			
Name:	Sizing 19 Sep 07:49	Net head [H]:	20 [m]
Location:	site-1	Max discharge [Q]:	20.0 [l/s]
		Frequency [f]:	60 [Hz]
		Max Turbine Power [P _{tm}]:	3 [kW]

Mechanical data

Turbine specifications		Generator specifications	
Turbine type:	Francis Turbine	Generator Type:	Asynchronous
Turbine layout:	Vertical	Number of poles:	4
Speed [n]:	1800 [rpm]	Frequency [f]:	60 [Hz]
Maximum RunAway speed:	2916 [rpm]	Power factor:	0.80 ~ 0.90
Specific speed [ns]:	91.82	Speed [n]:	1800 [rpm]
Blades number:	13	Peak Efficiency [η_p max]:	74.74 [%]
K:	0.51	Nominal Power [P _g]:	2 [kW]
Outlet diameter [D2e]:	118.89 [mm]	Other specifications	
Guide vanes height [Bd]:	13.00 [mm]	Runner weight:	0.02 [kN]
D01:	144.58 [mm]	Axial thrust:	0.44 [kN]
D0e:	173.12 [mm]	Total hydraulic thrust:	0.46 [kN]
NPSH:	0.57 [m]		
Z2:	9.59 [m]		
Pipe connection for valve DN:	92 [mm]		
Spiral case inlet diameter:	85.72 [mm]		
Peak Efficiency [η_p max]:	71.2 [%]		
Max Turbine Power [P _{tm}]:	3 [kW]		
Max Electrical Power [P] (async):	2 [kW]		
Flow @RunAway speed:	8.56 [l/s]		
Minimum flow:	1.76 [l/s]		

Q/Qmax	Efficiency
1.16	69.9
1.14	70.2
1.13	70.2
1.10	70.6
1.06	70.9
1.02	71.1
1.00	71.2
0.97	71.2
0.89	71.0
0.79	70.2
0.71	69.0
0.61	66.4
0.55	64.0
0.50	61.5
0.45	59.0
0.41	56.6
0.38	54.2
0.35	52.0
0.30	47.9
0.22	38.8
0.11	19.5
0.04	0.0

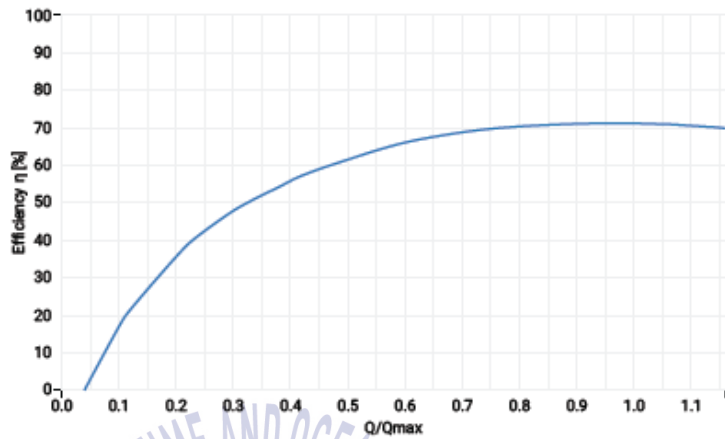


Figure 3.2 Turbine efficiency

Table 3.3 Inlet dimensions of the turbine

Diameter of runner	D_1	150	mm
Peripheral velocity	U_1	14.86	m/s
Meridional velocity	C_{m1}	2.33	m/s
Swirl velocity	C_{u1}	9.24	m/s
Blade angle	β_1	23	degree
Blade width	B_o	15.7	mm

Table 3.4 Outlet dimensions of the turbine

Diameter of runner	D_2	100	mm
Peripheral velocity	U_2	9.38	m/s
Meridional velocity	C_{m2}	2.34	m/s
Swirl velocity	C_{u2}	8.25	m/s
Blade angle	β_2	14	degree
Blade width	B_o	15.7	mm

Francis turbine is designed with 3 main components; spiral casing with 12 guide vane, 6 stay vane, runner, and draft tube are considered as per original dimensions to be manufactured. Turbine was designed following condition $H=20\text{m}$, $N=1800\text{min}^{-1}$ and $Q=0.02\text{m}^3/\text{s}$. The Unigraphics NX 8.5 software is used for modelling. The fluid domain is extracted from the structured model. Figure 3.3 shows the fluid domain of turbine.

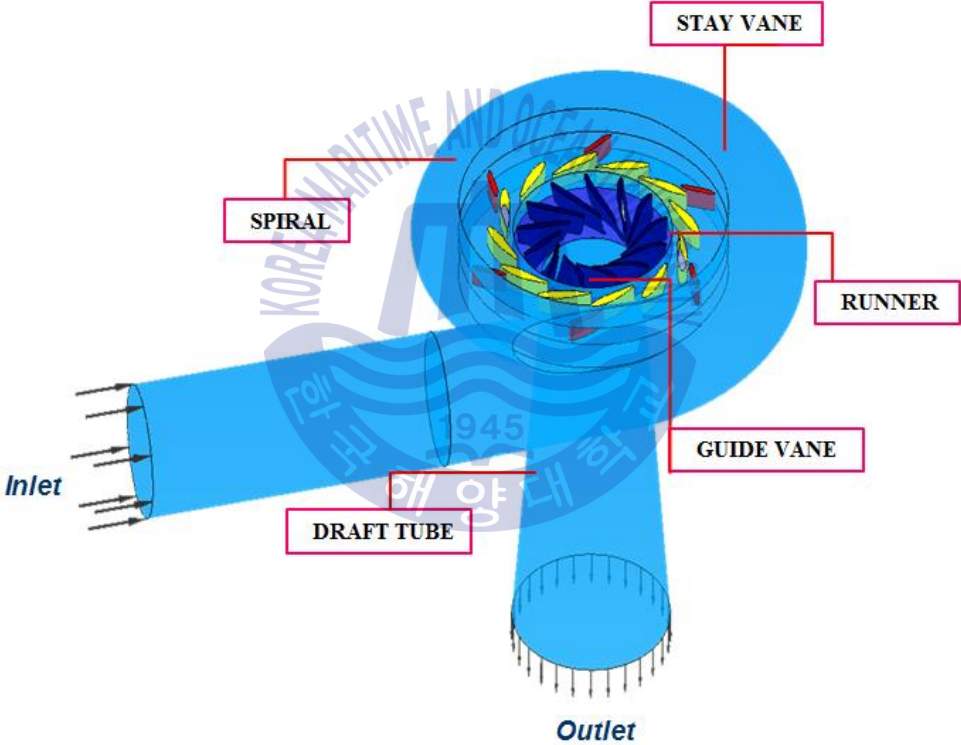


Figure 3.3 Modeling of the fluid domain of the turbine for CFD simulation

3.2 Numerical analysis

3.2.1 Computational fluid dynamics (CFD)

Computational fluid dynamics (CFD) is the study of fluid flow using computers to solve the governing mathematical equations that explains how fluids flows which otherwise is too complicated and impractical to solve by hand. As such, mathematicians have used the power of computers to tackle the problem. There are various industries that rely on CFD heavily, aerospace sector, military aircraft, auto motive sector and renewable energy sector. In addition to, computational fluid dynamics also is used in Bio-medical engineering which is a rapidly growing field and uses CFD to study the circulatory and respiratory systems. The following figure shows pressure contours and a cutaway view that reveals velocity vectors in a blood pump that assumes the role of heart in open-heart surgery.

Specialized CFD for the following systems:

- Multi-phase
- Heat transfer
- Interference of pipe line components: valves, pump, inlet/outlet etc.
- Bearing load assessment on flow components
- Coupled particle simulations modelling

CFD schemes for solving the full-potential solution of the Euler and Navier-Stokes equations. Fundamental equations of fluid dynamics is the continuity, momentum and energy equations.

1. Mass is conserved
2. Newton's second law
3. Energy is conserved

3.2.2 Grid discretization

The fluid domain discretization can be accomplished by multiple means, but the most often adopted in three-dimensional CFD are based on either tetrahedral or hexahedral volumes. A mesh that consists of mainly tetrahedral elements is referred to as unstructured mesh while a structured mesh is comprised of hexahedral elements. Ansys ICEM is used for numerical discretization of the domains [19]. In CFD simulation, there was always the big question of how fine mesh is needed to achieve a required level of accuracy. The mesh dependent CFD analysis was carried for the full domain and the influence of the mesh count on the efficiency is shown in Figure 3.4. Unstructured mesh was generated for the entire domain with the addition of prism layers on the wall boundaries to capture relevant boundary layer effects as shown in Figure 3.5. The total number of mesh nodes is also summarized in Table 3.5.

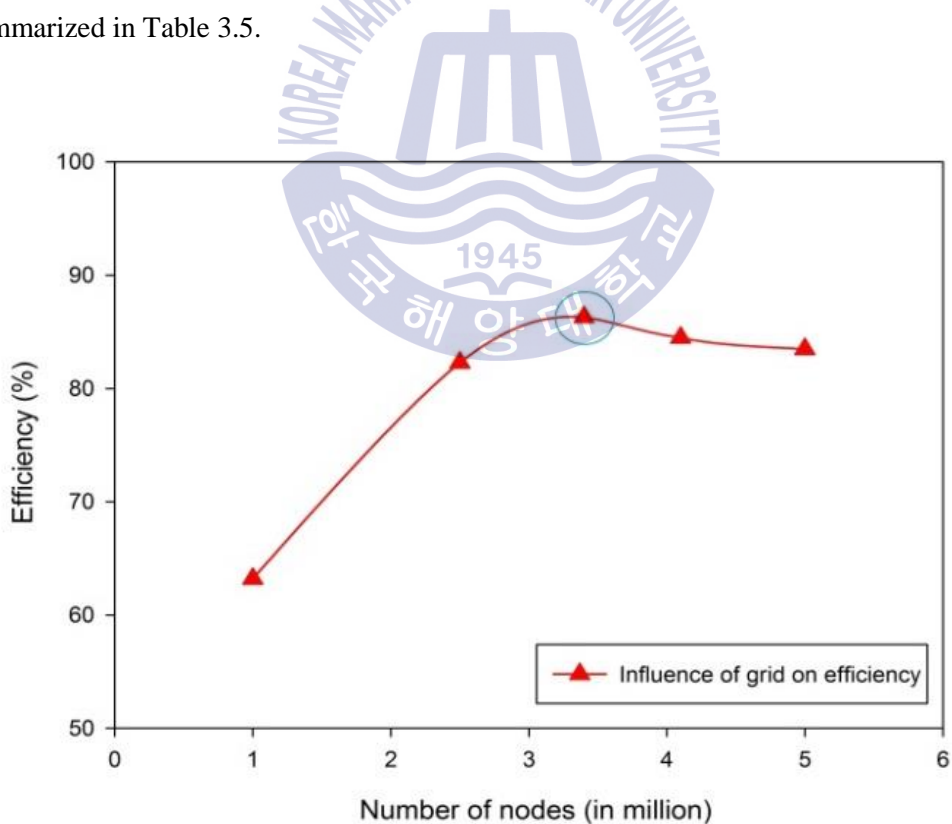


Figure 3.4 Mesh dependence

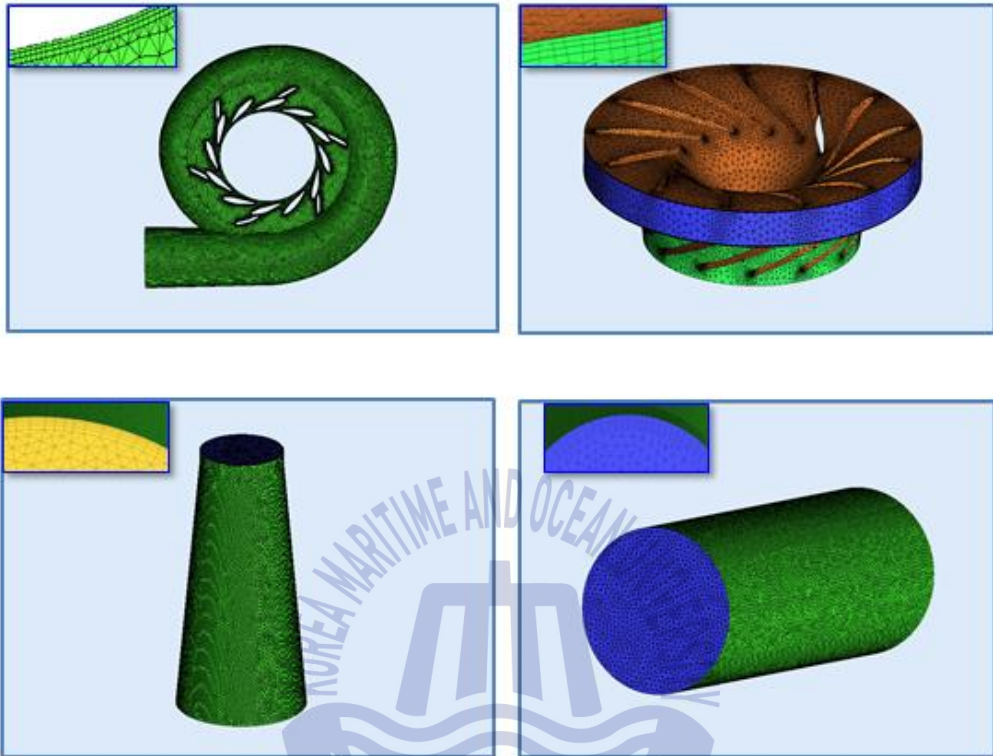


Figure 3.5 3D unstructured grids generation by parts for the computational domain.

Table 3.5 Summary of mesh data

Domain part	No. of nodes	No. of elements	Type of element
Casing (including stay vane and guide vanes)	179985	5997955	Tetrahedron
Runner	1349347	6064085	Tetrahedron
Draft tube	197717	90157	Tetrahedron

3.2.3 Boundary condition

Almost every computational fluid dynamics problem is defined under the limits of initial and boundary conditions. The simulation has been conducted by performing steady state Reynolds averaged Navier-Stokes 3D calculation at different operating conditions using Ansys-CFX 13 commercial solver. All CFD problems are defined in terms of initial and boundary condition.

The various parameters used in the equations depend on the type of boundary conditions used for the numerical simulation. Literature suggest different sets of boundary conditions for the CFD analysis of hydro turbines e.g. total pressure inlet & static pressure outlet, mass flow inlet & static pressure outlet [36]. Patel and Satanee [37] used mass flow inlet and pressure outlet boundary conditions for the numerical simulation of Francis turbine. Ruprecht et al [38] used mass flow inlet and outflow boundary conditions.

For the first set of boundary conditions: total pressure was defined at inlet of the casing and mass flow rate defined outlet of the turbine.

For the second case of boundary condition: Mass flow rate at the inlet of the casing as inlet boundary and pressure at the outlet of the draft tube as outlet condition.

The first set of the numerical simulation showed very high efficiency compared to the experimental data. The second set of the numerical simulation showed results that were accurate relative to the experimental data.

All solid walls have nonslip boundary condition. The rotational speed of runner 1800rpm. The entire model of the turbine is formed by combining the components with frozen rotor interface, each between casing and runner and runner and draft tube using General Grid Interface (GGI) method for mesh connection. Shear Stress Transport (SST) model is used for turbulence modelling.

6 different flow rates (over load, full load and part load) were used at a constant guide vane opening angle and constant rotational speed of 1800 rpm for the steady state analysis.

3.2.4 Hydraulic efficiency and power characteristic

The hydraulic efficiency is calculated using the relation which can be defined as;

$$\eta = \frac{T \times \omega}{(P_1 - P_o) \times \rho \times g} \quad (3.13)$$

Where:

P_1, P_o - Total pressure at inlet and outlet [Pa]

ω - Angular speed of runner [rad/s]

T - Torque produced by runner [Nm]

g - Gravitational acceleration [m/s²]

ρ - Density of water [kg/m³]

Available power is calculated using the relation which can be defined as;

$$P = \rho \times g \times Q \times H \quad (3.14)$$

g - Gravitational acceleration [m/s²]

ρ - Density of water [kg/m³]

Q - Flow rate [m³/s]

H - Head [m]

The hydraulic efficiency and power have been computed by equation (3.13) and equation (3.14). Different test cases were carried out by varying flow rate in which the best efficiency point was achieved at full load condition flow rate of $0.02\text{m}^3/\text{s}$. Table 3.6 and Figure 3.6 show result of the overall performance at different load condition. BEP is indicated as 3.32kW Power, 91.67% Efficiency at $0.02\text{m}^3/\text{s}$ flow rate. Power and efficiency drops at part loads due to loss in head in guide vane, runner and draft tube.

Table 3.6 Computational result at different flow rate

Cases	Flow rate (m^3/s)	Head (m)	Shaft power (kW)	Efficiency (%)
1	0.024	24.06	5.12	90.74
2	0.022	21.09	4.16	91.11
3	0.02	18.52	3.32	91.67
4	0.017	15.55	2.28	88.37
5	0.015	13.35	1.66	85.02
6	0.012	10.44	0.86	70.55

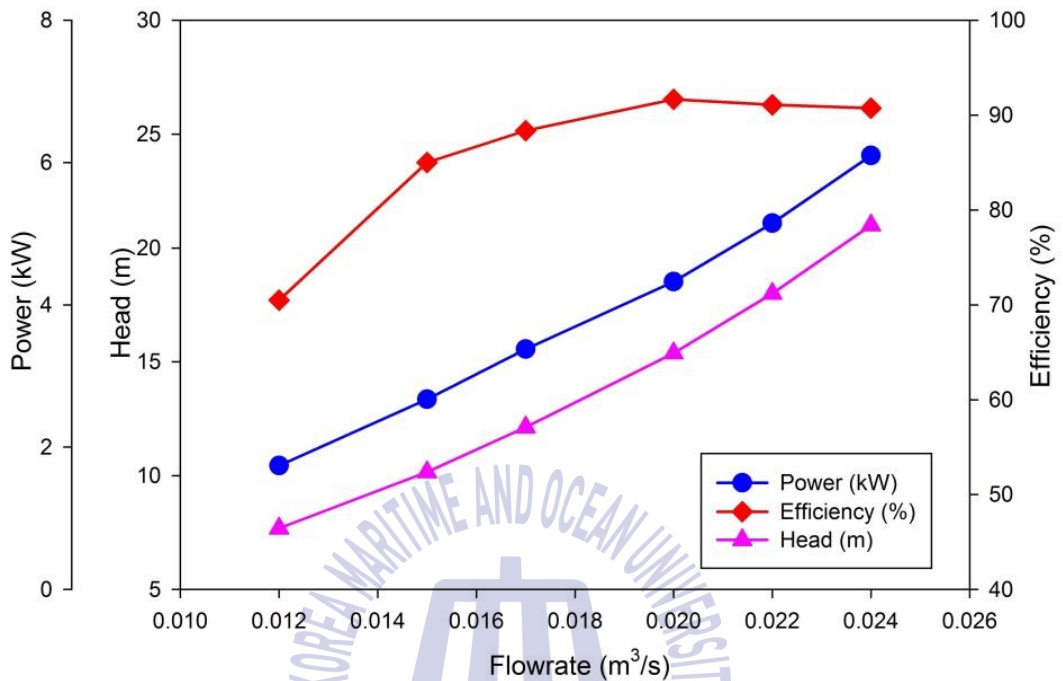


Figure 3.6 Variation efficiency, discharge and head at different flow rate

3.2.5 Flow feature and pressure distribution

Pressure difference from the pressure and suction sides are higher at higher loads. For all operating conditions, pressure distribution across the runner blades on the periphery of the rotor is not uniform. High pressure zones could be observed at the stay vane and guide vane regions which gradually decreased towards the inner radius. This means flow moves inward towards the runner. Maximum pressure is observed at the top of the runner and vice versa.. The pressure contour revealed a gradual decrease in pressure from inlet to outlet region on both pressure and suction side. The higher the operating load, the more the pressure difference across the blade. Pressure distribution on the runner at different flow rates is shown below in Fig 3.7.

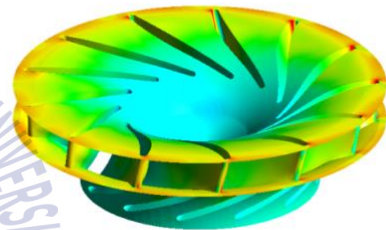
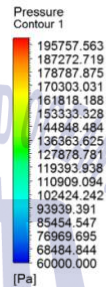
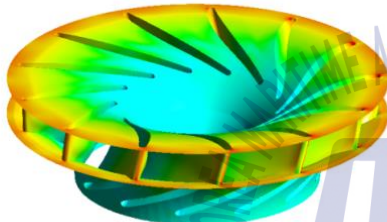
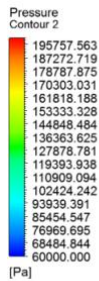
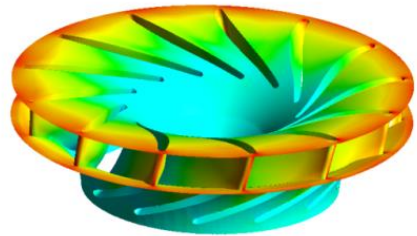
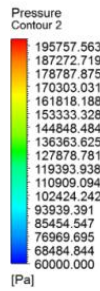
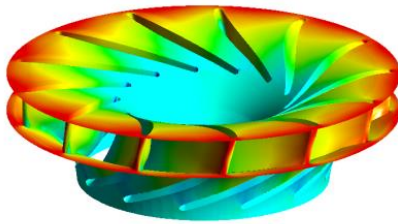
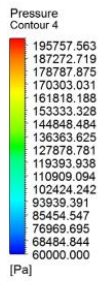
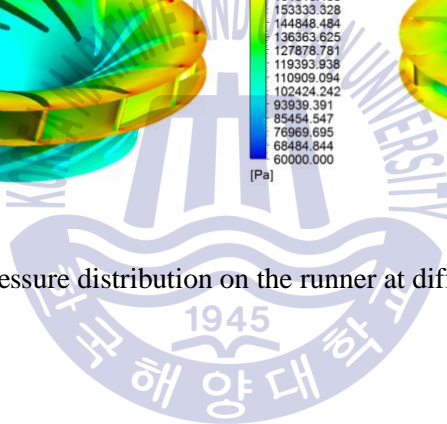


Figure 3.7 Pressure distribution on the runner at different flow rates



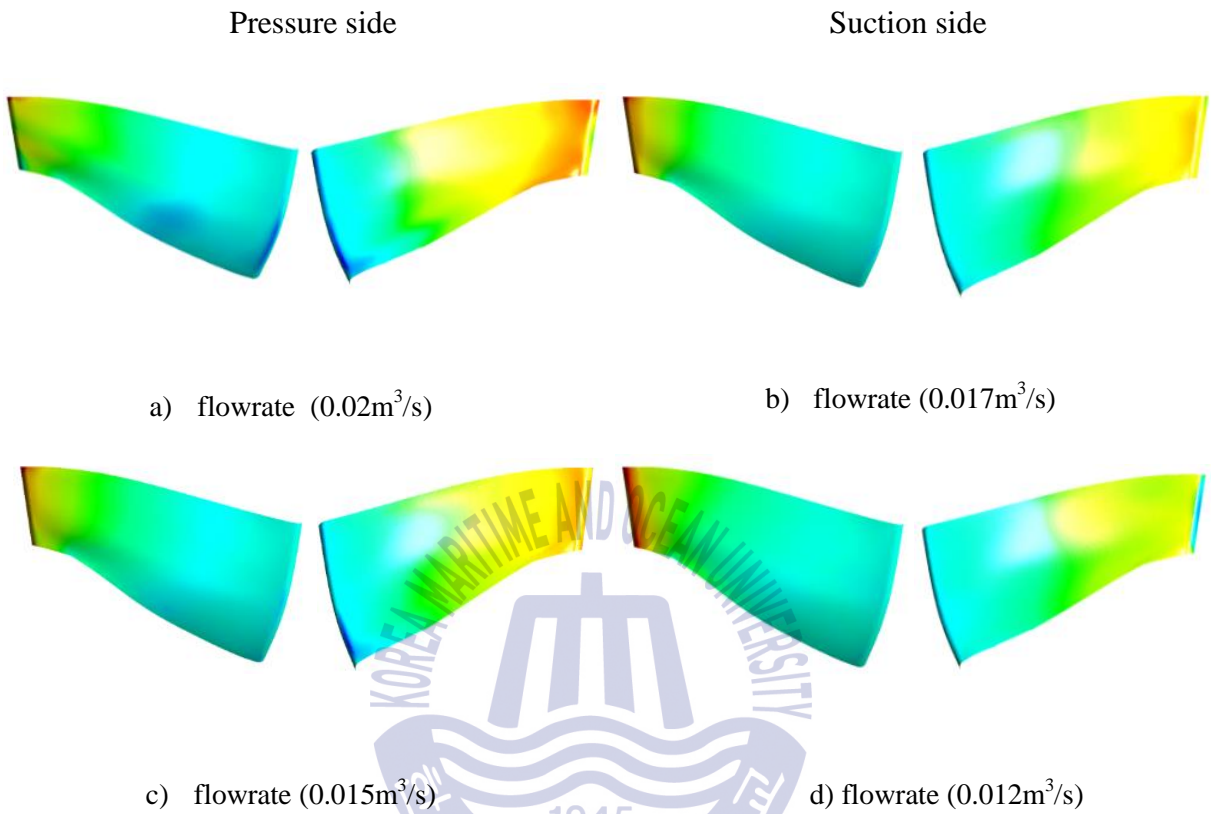


Figure 3.8 Pressure distribution on the single blade suction and pressure side

In aerodynamic and hydrodynamics, pressure coefficient as a dimensionless number is used to describe the relative pressure. Every point in fluid field has its own unique pressure coefficient [28]. Figure 3.9 and Fig 3.10 show the pressure coefficient on the single runner blade at different loads (over load, BEP and part load).

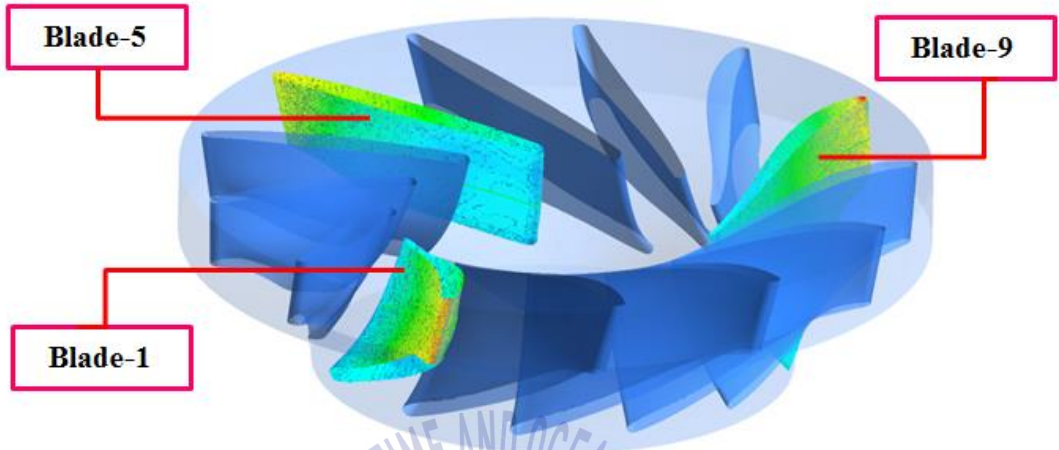
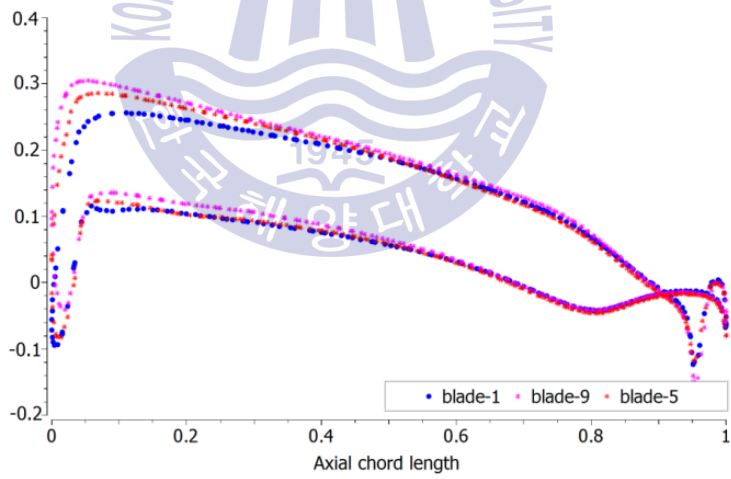
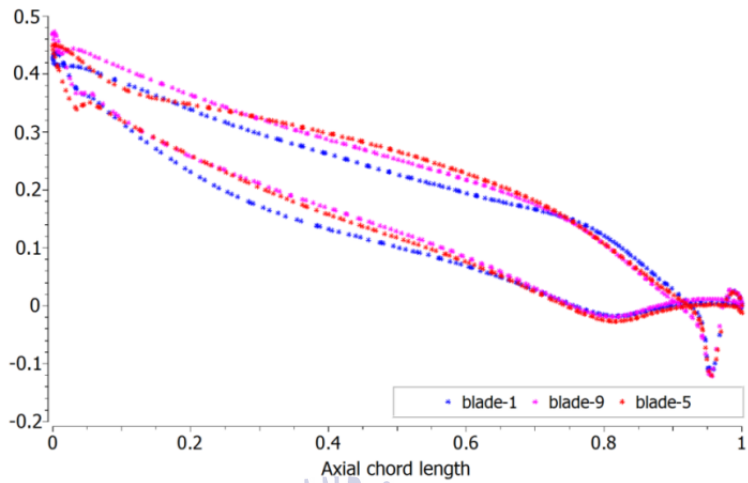


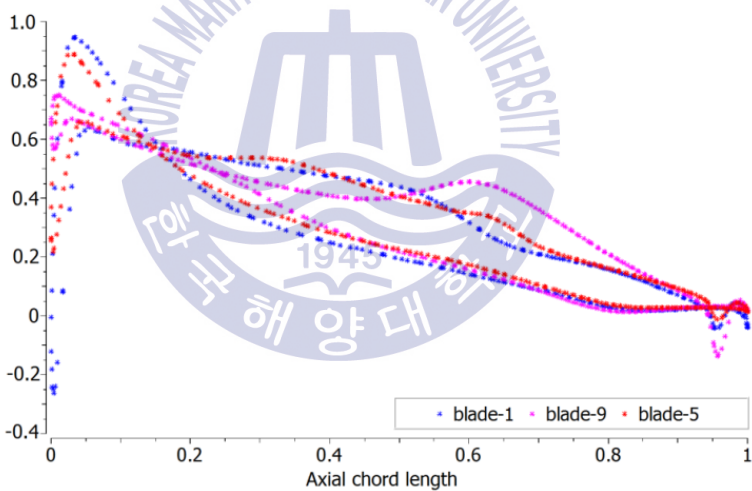
Figure 3.9 Francis runner



a) flow rate ($0.017\text{m}^3/\text{s}$)



b) flow rate (0.020m³/s)



flow rate (0.022m³/s)

Figure 3.10 Pressure coefficient of different single blades at different flow rates.

Velocity also increases gradually in the stream wise direction. Maximum velocity occurs near the guide vane. The separation of flow can be seen at the blade leading edge as shown in Fig 3.11 and Fig 3.12

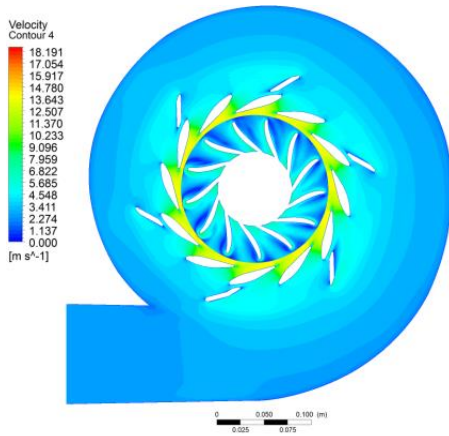


Figure 3.11 Velocity distribution in the spiral case at BEP

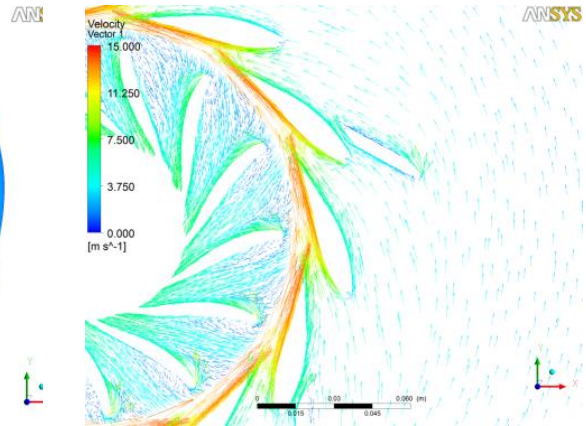


Figure 3.12 Velocity vector distribution in the spiral case at BEP

The draft tube is a necessary component installed in a reaction turbine. When turbine operates at partial load, hydrodynamic phenomenon observed causes severe flow instabilities and presence of vortex rope. The conical type draft tube is incorporated. Figure 3.13 shows the pressure distribution in the draft tube at different loads. The pressure distribution in the mid span of the draft tube at different flow rates is indicated in Fig 3.13. It can also be observed that the pressure gradually increases towards the outlet of the draft tube.

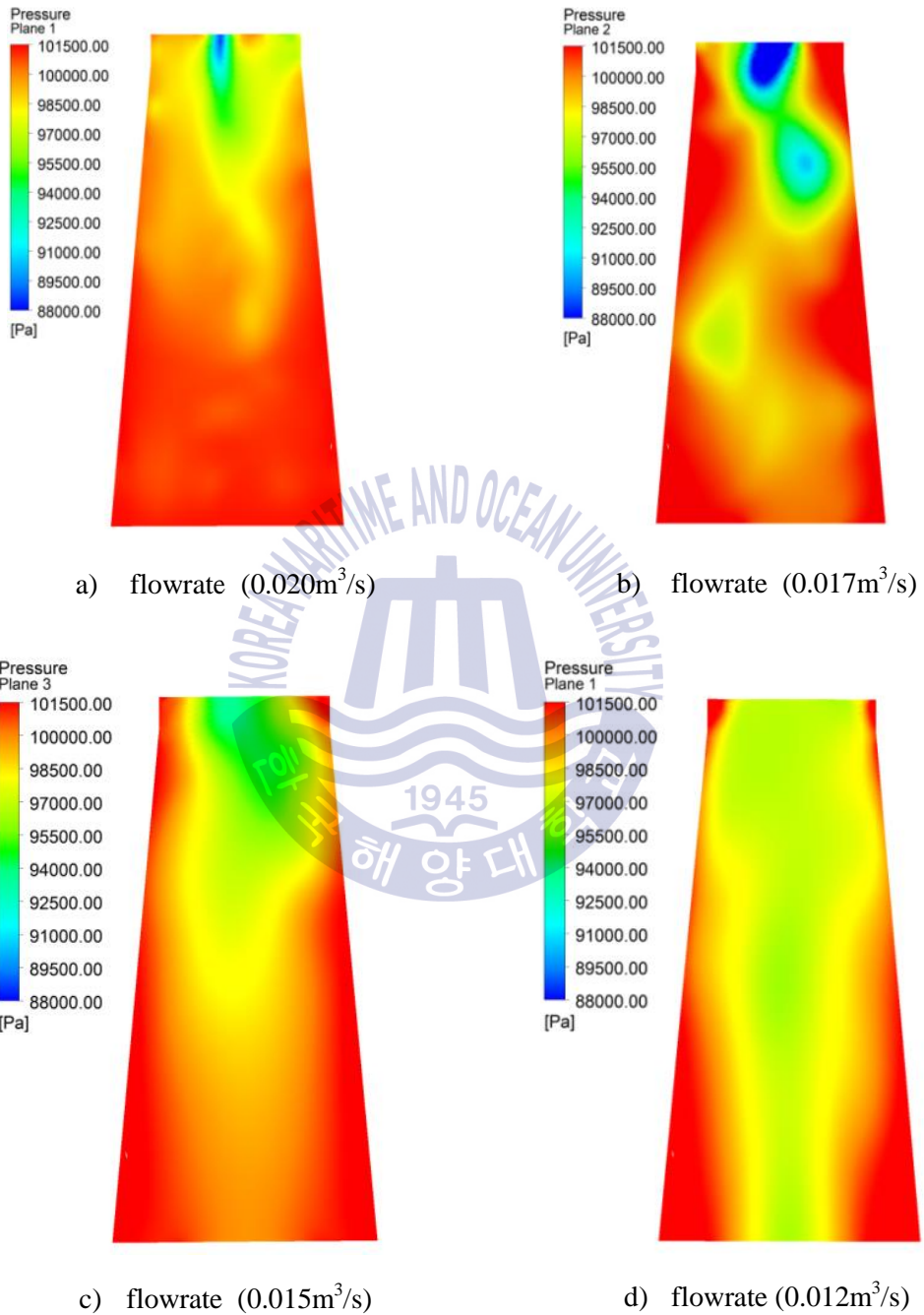


Figure 3.13 Pressure contour in the draft tube by different flow rate

3.3 Unsteady flow analysis

3.3.1 Unsteady flow at full load

The first order of simulation is showed in the Chapter 4. The second order for simulation method is based on multiphase transient flow in operating range from part load to full load and steady state results used for initial condition. Reference Pressure=0 Pa, Vapor pressure = 3169 Pa (temperature at 25°C). For the transient analysis the time step was set as 0.0001833s corresponding to a runner rotating angle of 2° per time step. Total computational time was 0.18s for 10 rotational periods of the runner.

Pressure decreased due to flow acceleration as shown in Fig 3.14. The flow velocity increases gradually from the inlet of the turbine to exit due to the guide vanes, kinetic energy of high-speed fluid is transferred into pressure energy, and velocity becomes lower when fluid goes into the runner blades.

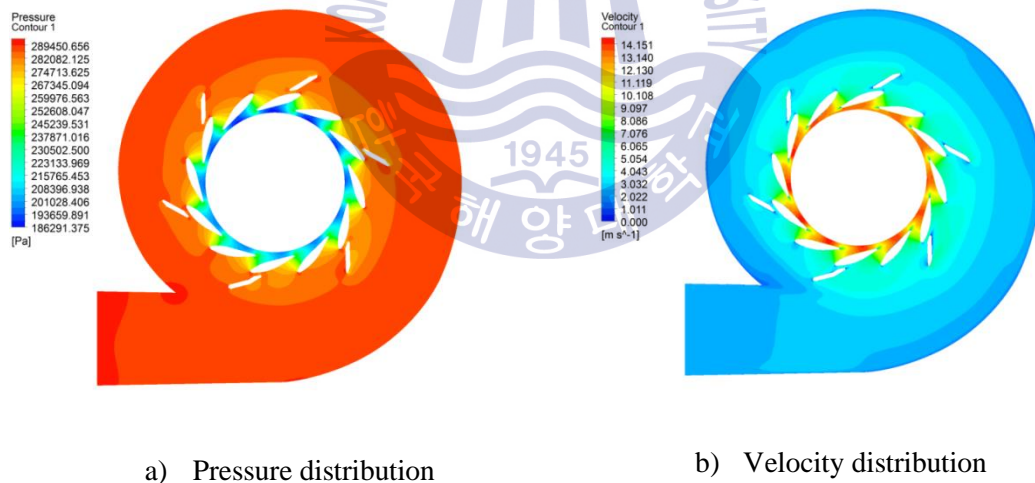


Figure 3.14 Unsteady flow in the mid span of spiral casing

Figure 3.15 shows the relative velocity vector in the middle of the spiral casing. There seems large incidences at the leading and tailing edge where flow mixing occurs.

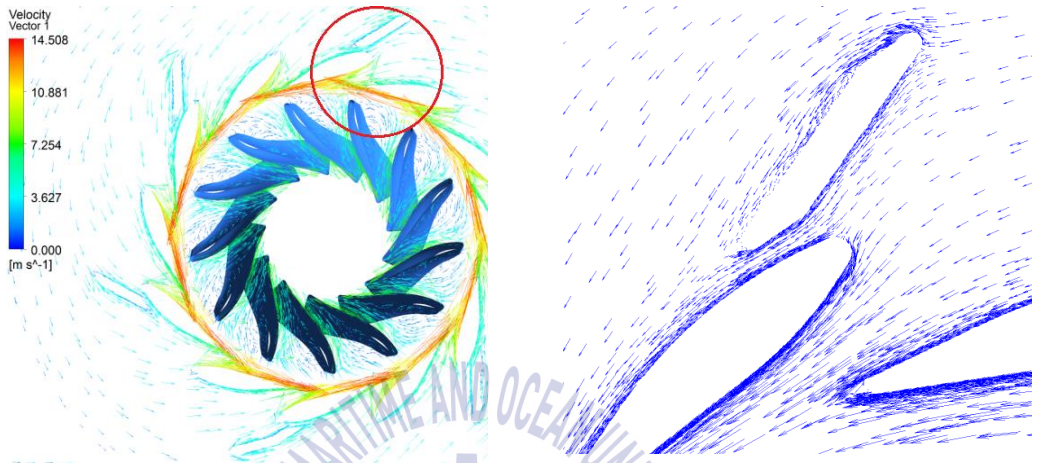
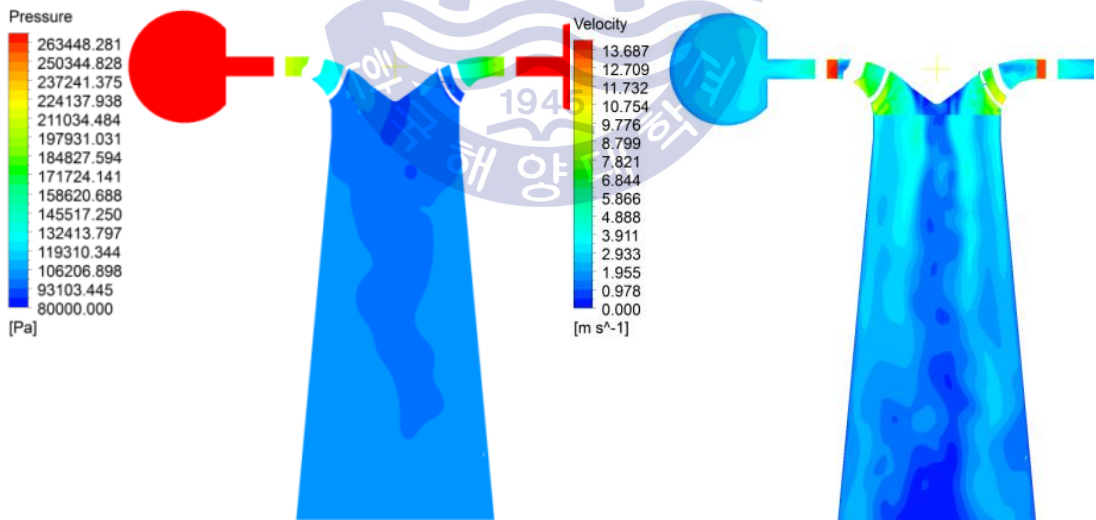


Figure 3.15 Velocity vector distribution at the spiral casing



a) Pressure contour

b) Velocity contour

Figure 3.16 Flow characteristics over the whole domain at full load

Pressure contour and Velocity contour respectively describes the flow structure inside as shown in Fig 3.16. Operation of hydraulic turbines in some off-design conditions exhibit local pressure pulsation caused by rotor-stator interaction and draft tube vortex precession that propagate along the whole water conduit [32]. A corkscrew shaped non-cavitating positive vortex was obtained at the inlet of the draft tube whose magnitude and strength changed with the runner rotation. The draft tube vortex appears at partial load operating regimes, usually in radial turbines and also at single regulated axial turbines [33]. Figure 3.17 shows the average torque of the runner blades at full load condition.

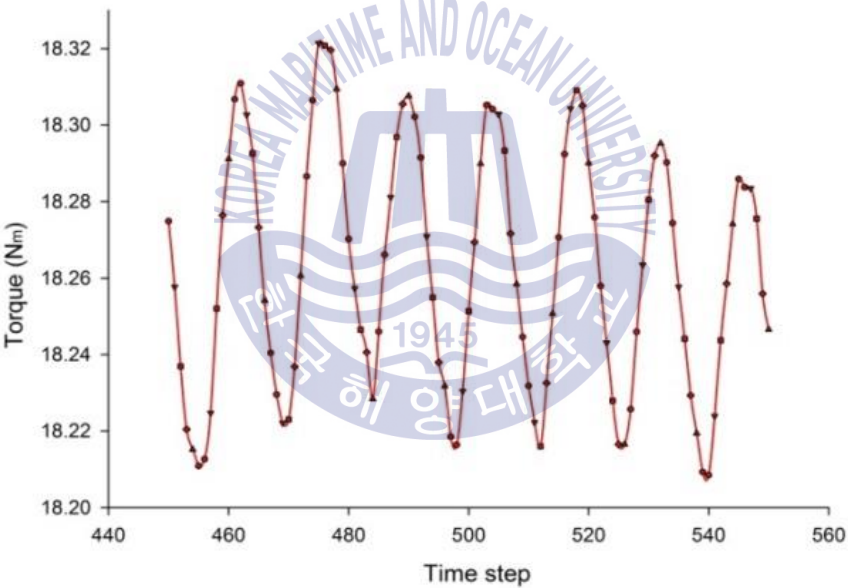


Figure 3.17 The average torque distribution at runner

The rotor-stator interaction between guide vanes and runner always induces pressure fluctuation inside the runner. The measurement of the pressure oscillations caused by vortex rope is discussed in [34].

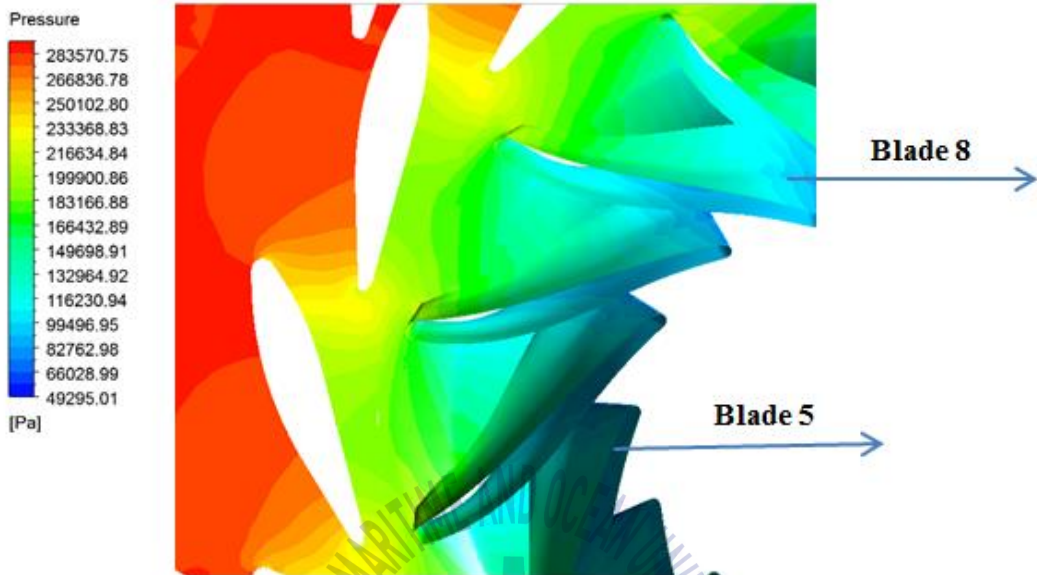


Figure 3.18 Pressure distribution on the spiral

Figure 3.19 shows the torque distribution of 2 runner blades. Periodic distribution of torque as time step increases. All blades have different phase and ultimately, sum of forces remain constant. Fluctuation caused by guide vanes is small and wake regions vanish quickly due to accelerated flow.

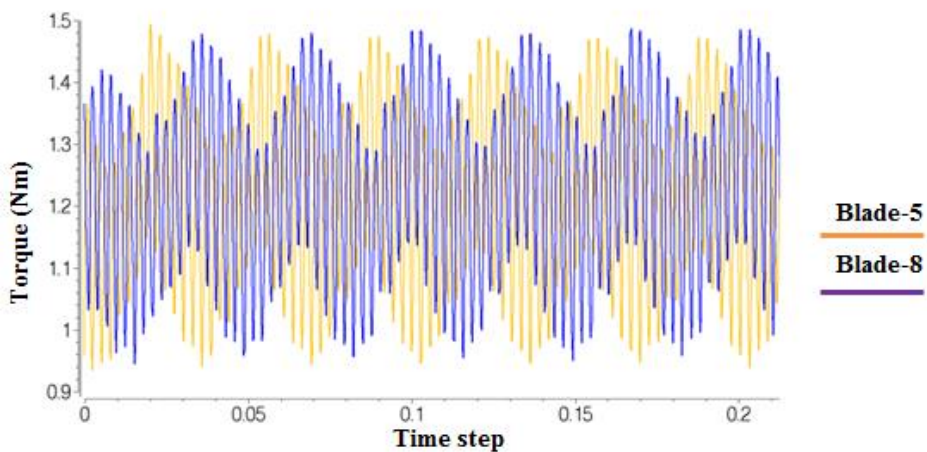


Figure 3.19 Torque distribution in the runner blade

The static pressure and velocity streamline distribution on single blade are represented in Fig 3.20 and Fig 3.21. The maximum pressure is located at the leading edge of the blade.

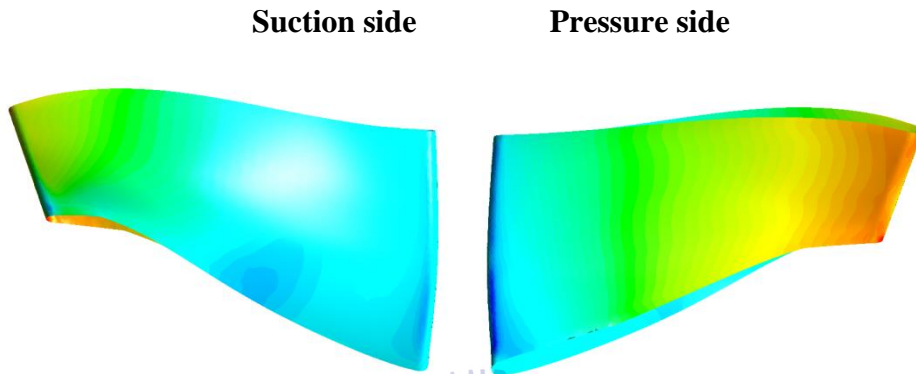


Figure 3.20 Pressure distribution in the runner blade

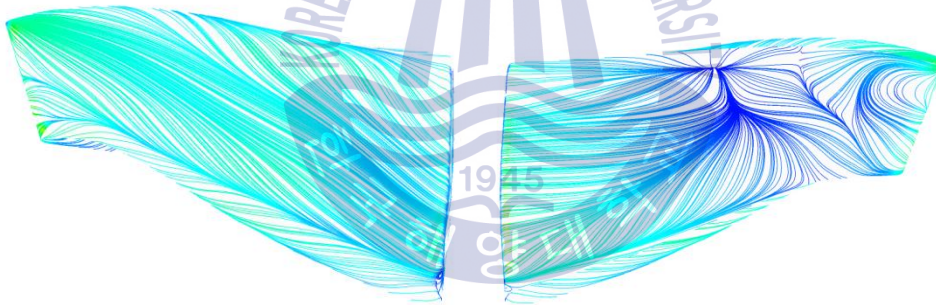


Figure 3.21 Velocity streamline in the runner blade

3.3.2 Unsteady flow at partial load

The flow analysis of the draft tube of hydraulic turbine is of practical interests for either the design of new machines or the rehabilitation of existing ones. The specific pressure energy recovery in the draft tube affects significantly the efficiency and power output of the machines at high discharge. Also, the hydraulic turbines which operate under a wide range of heads and outputs, are subjected to considerable pulsating pressures at off design

conditions produced by a vortex rope in the draft tube that could lead to pressure surges in the hydraulic system.

At part load the transient flow was characterized by the rotating vortex rope in the draft tube cone. This effect could be observed by the high measured values on the suction side of the runner blades near to the trailing edge

3.3.3 A draft tube swirl

At part load operation of the turbine swirling flows appears downstream the runner which produces vortex rope [20-24]. Several major difficulty phenomena are pressure pulsation, axial and radial forces, torque fluctuation, structure vibration developed by vortex rope. These factors are responsible for the efficiency reduction, noise, vibrations, variations in power output, vertical movement of the runner, and pressure pulsations in the draft tube.

3.3.4 Vortex rope in part flow

In this study, SST turbulence model was used to predict the occurrence and nature of vortex rope which is responsible for curving the streamlines. To appropriately capture formation of the vortex rope, the time step was set to 10 times the runner cycle time. When a blade passes in front of a guide vane, it receives a hydrodynamic force.

Numerically obtained shape of draft tube vortex and its accuracy largely depends on the choice of the turbulence model used for the simulation. Figure 3.22 illustrated difference of the turbulence model.

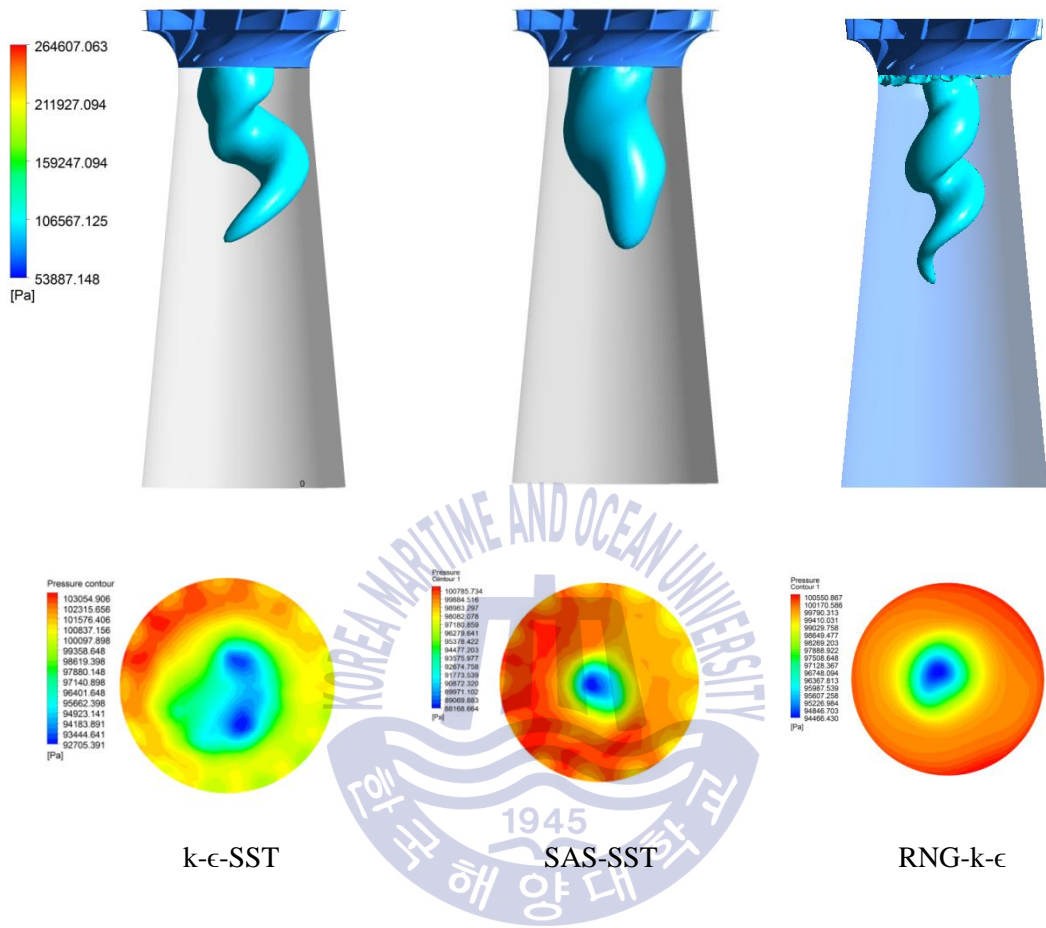


Figure 3.22 Effect of turbulence model on shape of vortex rope

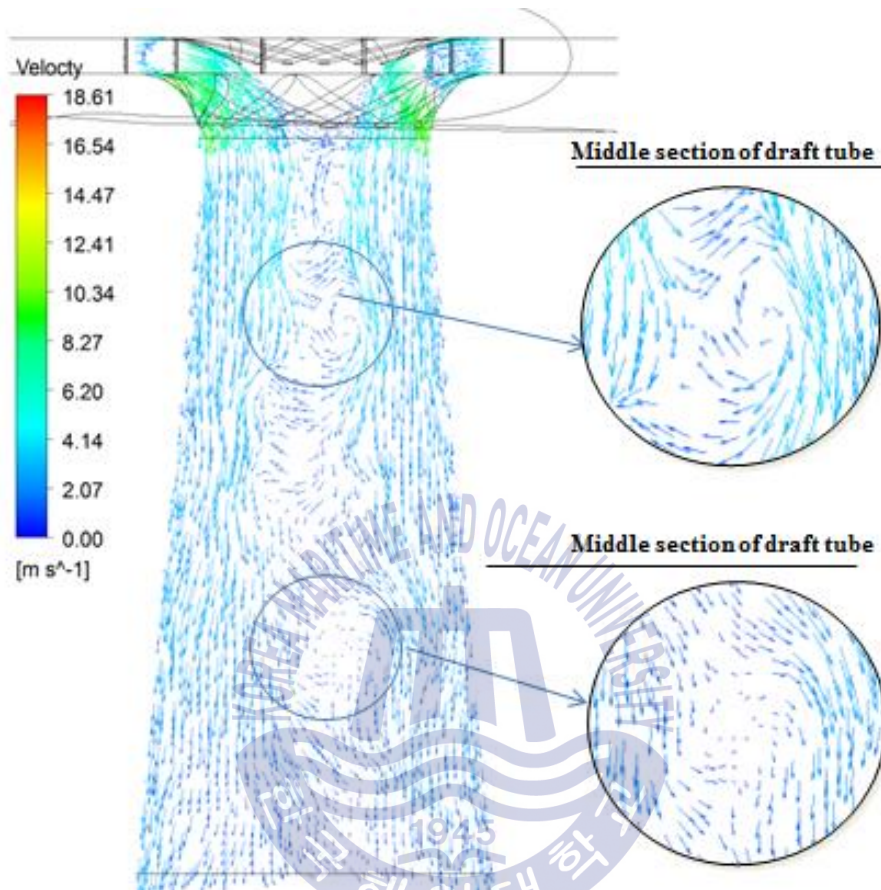


Figure 3.23 The vector field in the draft tube

As illustrated in Fig 3.24, the recirculation of the working fluid in the mid -section due the loss of flow.

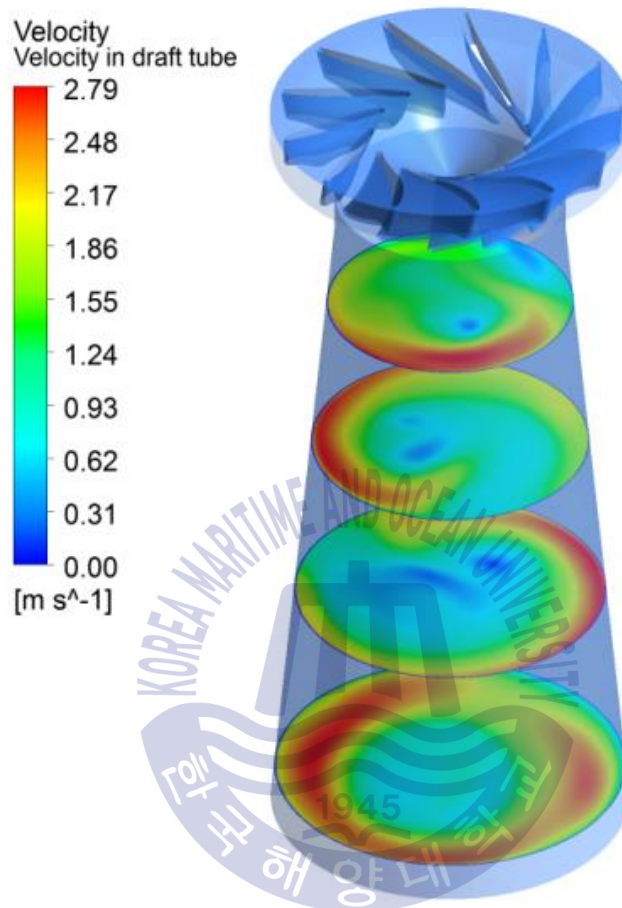


Figure 3.24 Velocity distribution in the draft tube

As shown in Fig 3.25 and Fig 3.26 distribution of pressure and velocity vector in the mid-section of draft tube at a different instance of runner rotation.

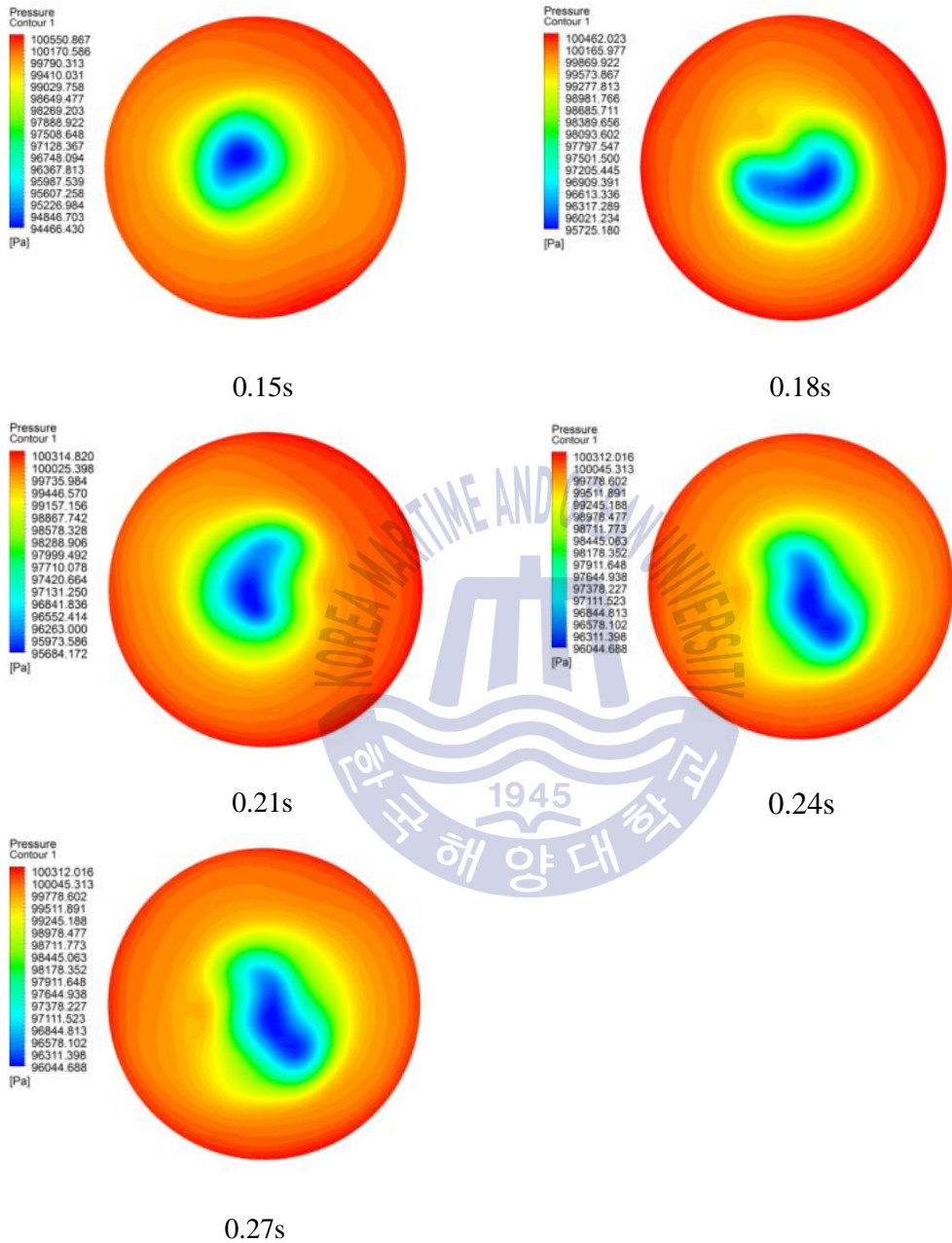
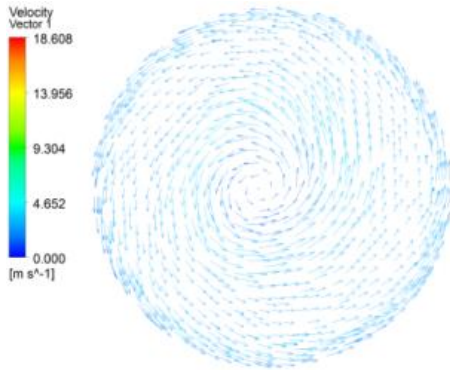
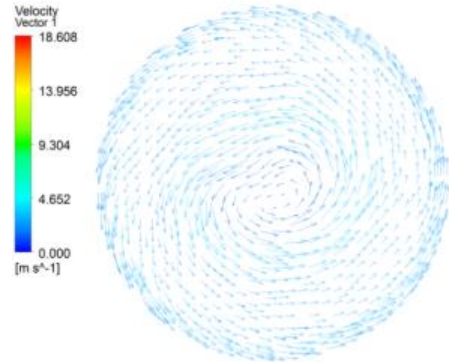


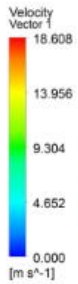
Figure 3.25 Pressure region in mid-section of draft tube



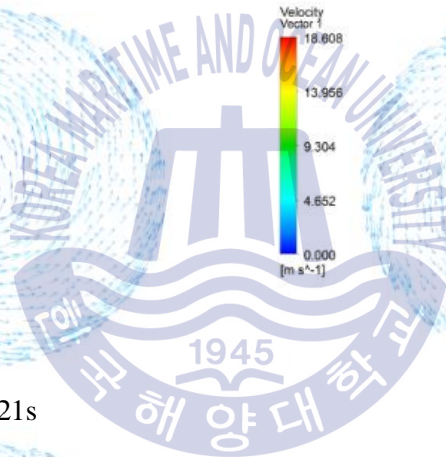
0.15s



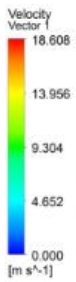
0.18s



0.21s



0.24s



0.27s

Figure 3.26 Velocity vector region in mid-section of draft tube

3.4 Signal analysis

Vortex rope interacts with the turbine components to produce low frequency pulsations. This causes vibration and hydraulic loss. Time-varying pressures recorded at 8 different points in the casing, runner and draft tube. FFT was carried out to analyze pressure fluctuation signals.

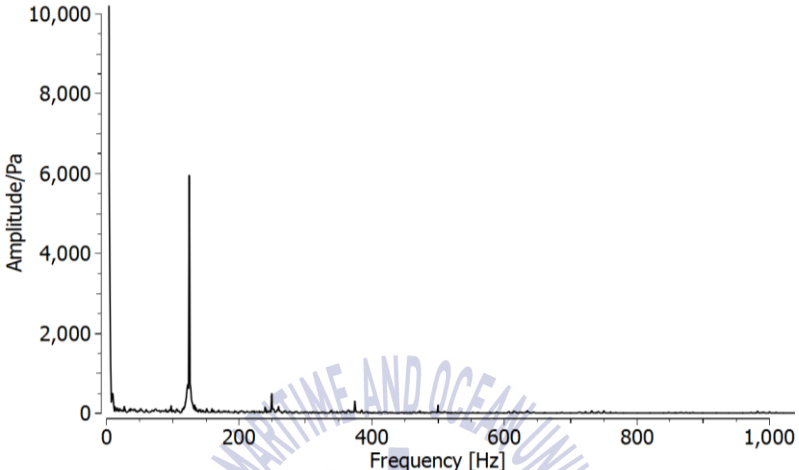


Figure 3.27 Pressure recording locations

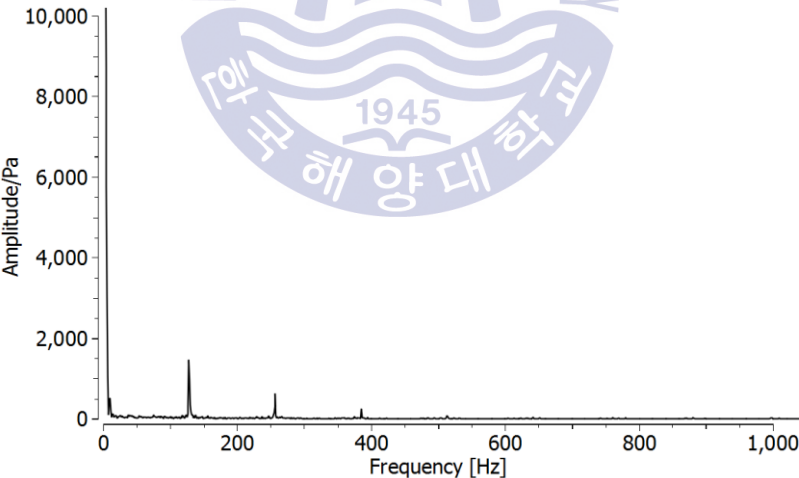
The vibration level at the spiral casing, runner blade and in the draft tube as shown in Fig 3.27 was found to be of similar magnitude. The level of vibration in the runner blade is relatively higher than that in the casing and draft tube.

The interaction between the rotating component and stationary components of Francis turbine is a common phenomenon during its operation but the effect is manifested more in medium to high head machines. With turbines operating at medium head and above, the velocity of the flow at the exit of the guide vanes are large with small radial gap between the blade rows which results in significant pressure fluctuation with respect to the stress levels. Since the flow field in the radial space between the guide vanes and runner is non-uniform circumferentially, the static inflow pressure, the magnitude of velocity and the

flow angle passing through each runner channel also vary circumferentially, creating an unsteady load on the blade [35].

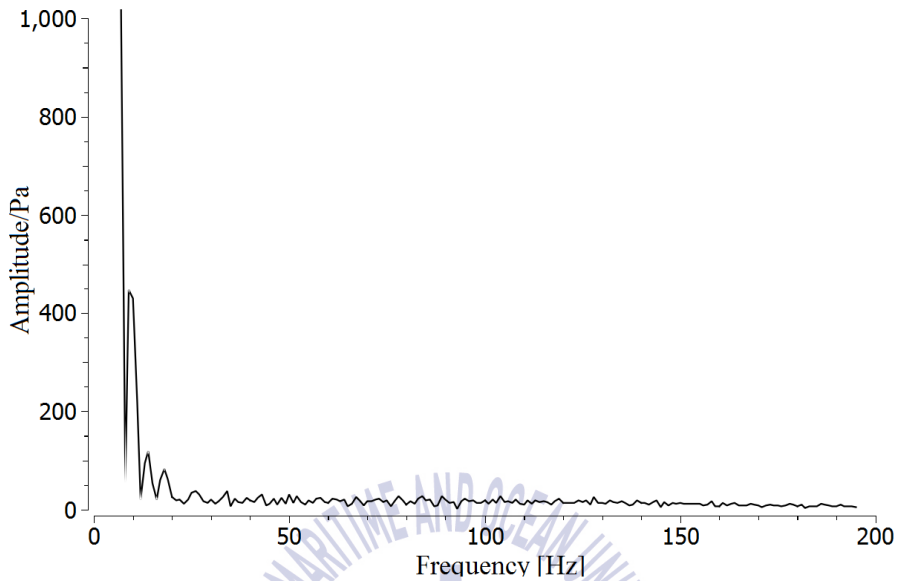


a) blade pressure side

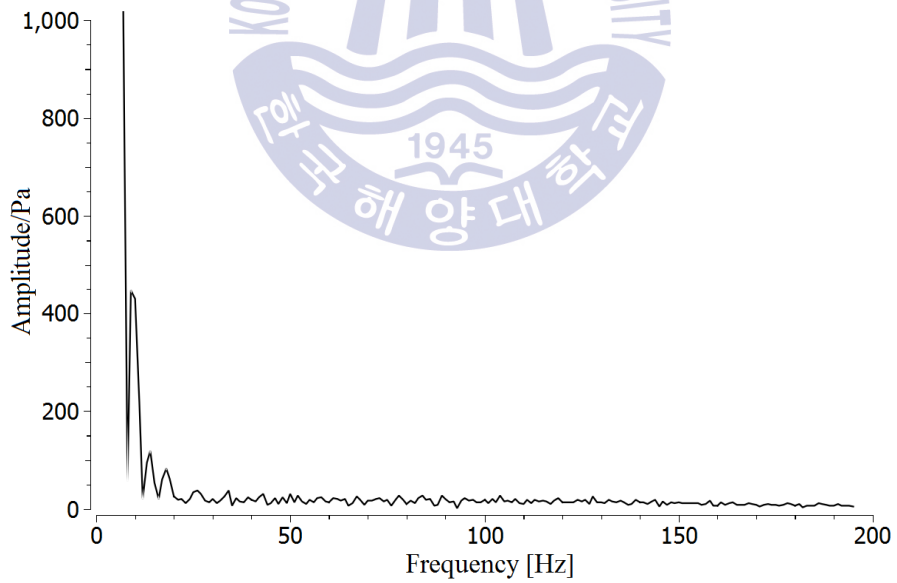


b) blade suction side

Figure 3.28 Amplitude spectra in runner blade



a) PD1 point



b) PD2 point

Figure 3. 29 Amplitude spectra in draft tube

3.5 Misaligned guide vane

Pressure pulsation is the primary reason for unstable operation of any hydro machinery. Misaligned guide vane have been keenly incorporated in pump turbine system to improve flow stability and minimize the pressure pulsation [26-29]. In this study, I was trying to understand characteristic of the dominant unsteady flow frequencies in the entire flow passage of the Francis turbine for various misaligned guide vane openings.

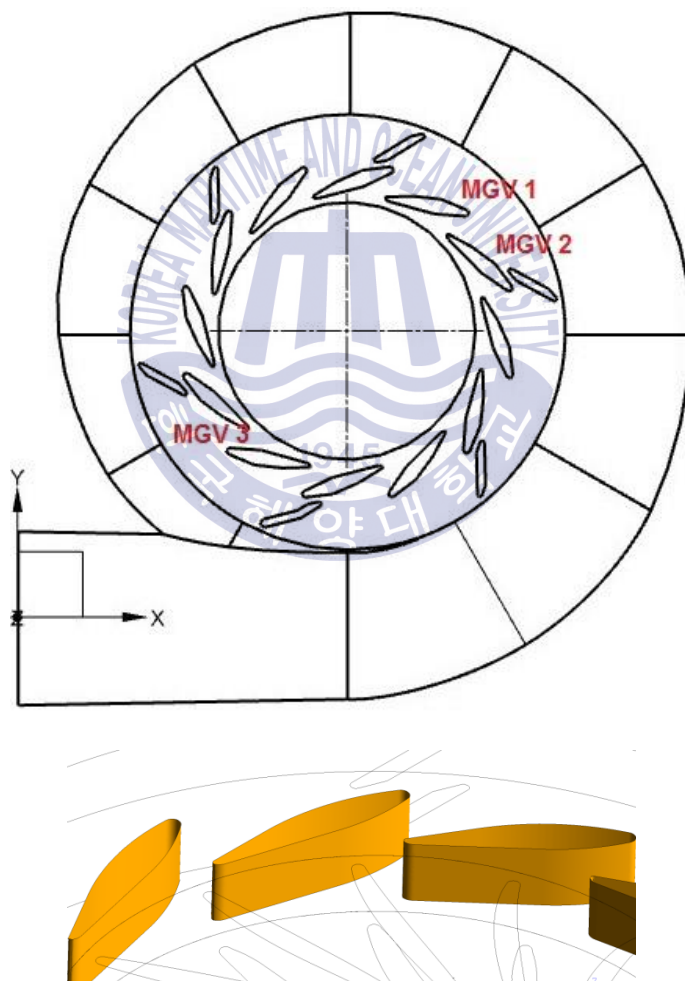


Figure 3.30 MGV position

The guide vane angle of turbine under study is $\alpha_1=26.5$. The 3 different opening angle of 25° , 28° and 30° were chosen for analysis as shown Fig 3.30. For this calculation, structured and unstructured meshes were selected for spiral casing runner and guide vane. The time dependent numerical analysis was conducted followed by steady state simulation with the same setting 24° of guide vane angle carried out for the transient analysis, the time step 2° of runner was taken 10 full rotation. So time step was 0.0000185s, corresponding to 1/80of the runner rotation period.

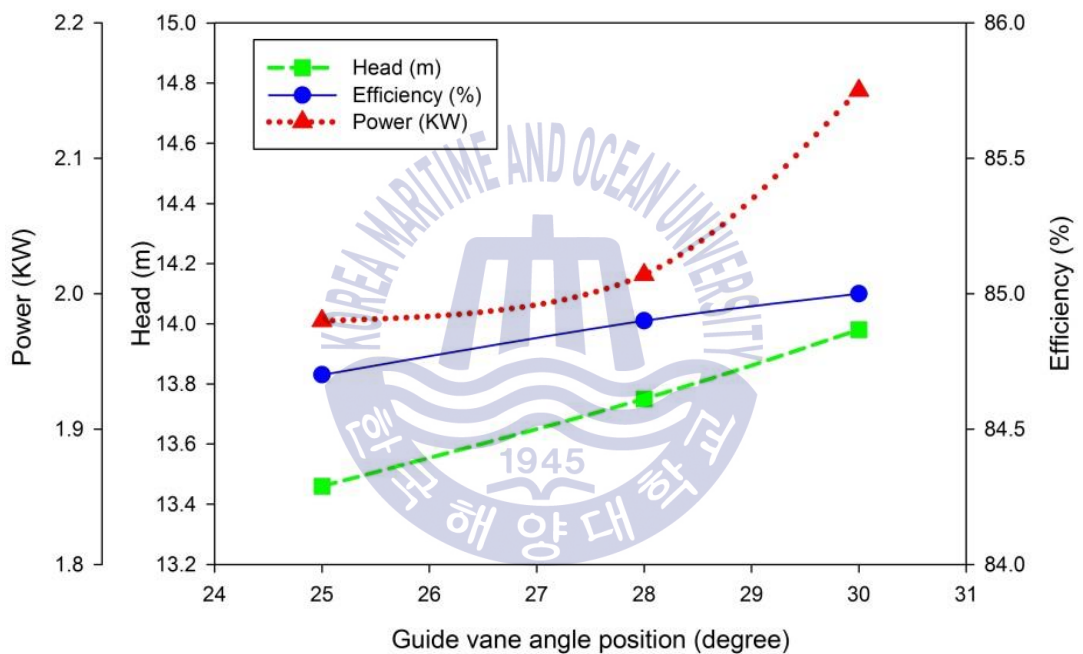


Figure 3.31 Variation efficiency, discharge and head at different guide vane angle

Figure 3.31 shows the result of calculation. The increasing MGV opening increased the flow area inside the guide vanes which increased the discharge, the power and the hydraulic efficiency.



With MGV

Without MGV

Figure 3.32 Influence of MGV on shape of vortex rope

CHAPTER 4. EXPERIMENTAL ANALYSIS

4.1 Experimental setup

The experimental values used for comparison and validation in this thesis. This executed at the test rig at the Flow Informatics Laboratory in Korean Maritime and Ocean University. The experimental setup designed for this study is an open loop setup with the draft tube connected to a downstream tank open to air. The setup consist of a water tank, Francis turbine, hydro cyclone separator (hydro cyclone separator did not used to experimental), 2 pumps, valves, electromagnetic flow-meter, flow straightener, torque transducer, powder brake, VFD, and pipe lines. The water supply pumps (pump1, pump 2) set draws water from the main tank and supplies it to turbine. The corresponding values for each rated discharge and head of pumps $1\text{m}^3/\text{s}$ and 29 m respectively at 1750 rpm. Pump 1 have provide to the flow to Francis turbine only when the performance analysis of the turbine is required to be done. Similarly, to get the performance analysis of the Francis turbine with the separator in-line both pumps have to be operated simultaneously. [Atmaram Kayastha]. Main valves are provided right in front of pump 1 and pump 2 in connection to the water tank while the auxiliary valve is installed in between separator and pump 1. A turbine assembly is consist of spiral casing, a bearing pedestal, a rotor assembly of shaft, gunmetal runner and brake drum all mounted on a suitable sturdy base. Guide vanes are provided in the turbine to regulate the flow into the runner. The guide vane opening adjustment is made through a hand wheel by a suitable link mechanism. A conical draft tube is connected to the turbine outlet by a flexure. Figure 4.1 shows the experimental setup.

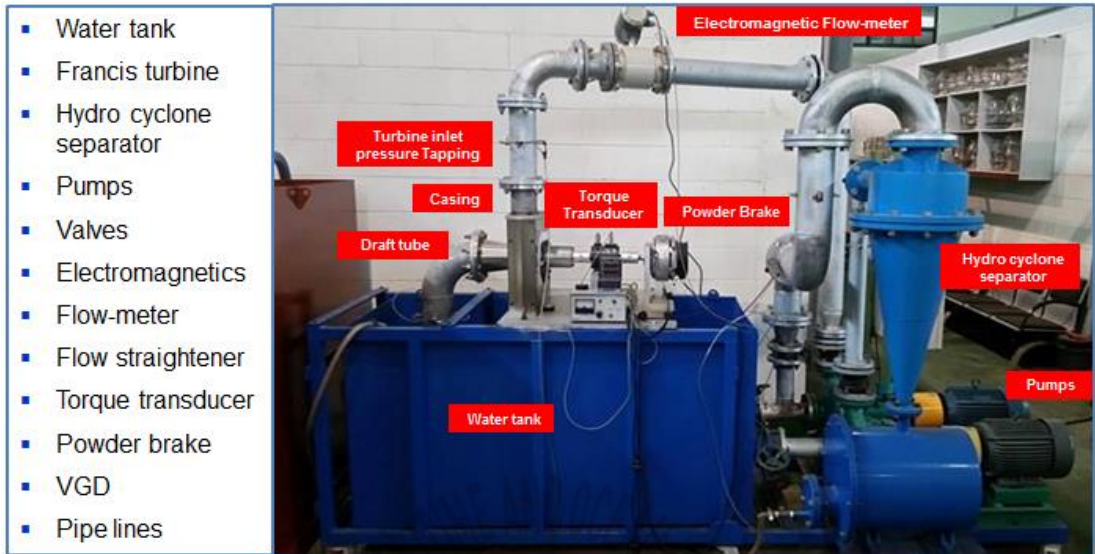


Figure 4.1 Experimental setup

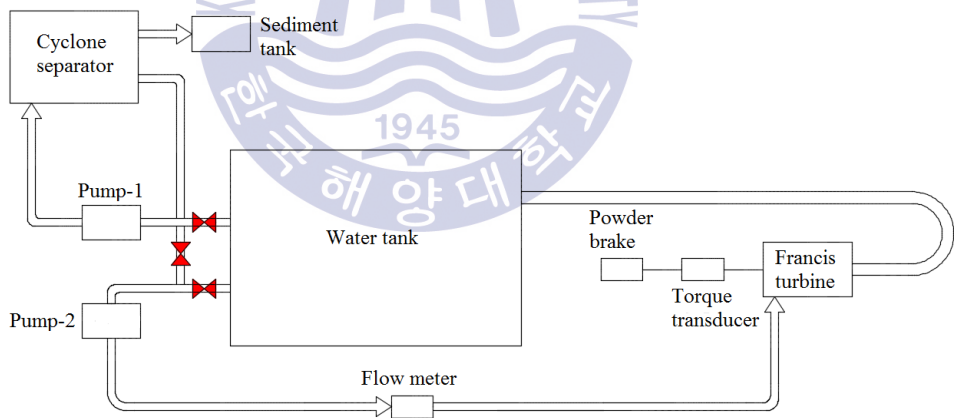


Figure 4.2 Experimental schema of Francis turbine

4.2 The experimental apparatus specifications

4.2.1 Torque Transducer

A torque transducer is sensing unit for measuring torque on a rotating system. The use of strain gauge with brush and slip ring in transducer include test of motor power, test of load speed reducers, test of brakes and clutches, test of nut and bolt tightening torque calculation and also test of brake properties. The torque transducer consist of shaft open at both ends. One end of the shaft was coupled to the powder brake shaft while other end was coupled to the turbine shaft. A flexible jaw coupling was used to couple the shafts. Jaw coupling are designed to transmit torque while damping system vibrations and accommodating misalignment which protects other components from damage [30].

SBB-5K number of model torque transducer used for experimental as we shown in Fig 4.3 in Table 4.1 and table 4.2 shown the specification of torque transducer.



Figure 4.3 Shaft type torque transducer

Figure 4.4 illustrates schematics of the torque transducer.

Feature:

- With RPM sensor
- Continuous torque measurement of a rotating object
- Strain gauge method with high precision using brush and slip ring

Dimension:

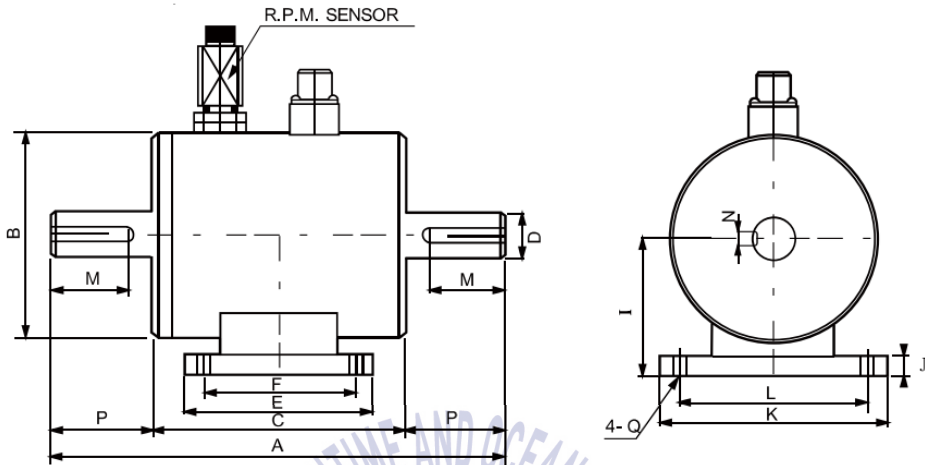


Figure 4.4 Schematics of the torque transducer

Table 4.1 Dimension of torque transducer

Capacity	A	B	C	D	E	F	I	J	K	L	M	N	Q	P
5-10kgf-m	220	110	130	23	105	85	70	10	120	100	36	7	9	45

Table 4.2 Torque transducer specification

Rated capacity	5kgfm-10kgfm
Rated output	1.5mV/V \pm 1%
Nonlinearity	01% of R.O
Hysteresis	01% of R.O
Repeatability	01% of R.O
Terminal resistance input	350 \pm 1%3.5 Ω
Terminal resistance output	350 \pm 1%3.5 Ω
Insulation	200 M Ω
Temperature Range Compensated	0.3% R.O/10 $^{\circ}$ C
Temperature Range Safe	0.2% R.O/10 $^{\circ}$ C

Excitation Recommended	10V DC
Safe overload	150% R.C

4.2.2 Powder brake

An electromagnetic braking device is also known as powder/ particle is used in the experimental analysis to apply load on the turbine and dissipate the power generated as heat energy. Magnetic particle brakes are unique in their design from other electro-mechanical brakes because of the wide operating torque range available. Like an electro-mechanical brake, torque to voltage is almost linier; however, in a magnetic particle brake, torque can be controlled very accurately (within the operating RPM range of unit).

Magnetic particles (very similar to iron filings) are located in the powder cavity. When electricity is applied to the coil, the resulting magnetic flux tries to bind the particles together, almost like magnetic particle slush. As the electric current is increased, the binding of the particles becomes stronger. The brake rotor passes through these bound particles. The output of the housing is rigidly attached to some portion of the machine. As the particles start to bind together, a output shaft. When electricity is removed from the brake, the input is free to turn with the shaft. Since magnetic particle powder is in the cavity, all magnetic particle units have some type of minimum drag associated with them [30]. The model number of the powder brake used in the analysis is PRB-5Y₃F. The powder brake was coupled to the torque transducer using jaw coupling. The specifications of the powder brake given in the Table 4.3 and Fig 4.5.



Figure 4.5 Powder brake

Table 4.3 Specification of Powder Brake

Model	PRB-5Y ₂ F	Unit
Torque	50	Nm
Voltage	24	DC V
Current	3.5	A
Power	84	W
Powder Quantity	80	g
Rev count	800	rpm
Rate of slip production	1500	W
Bearing specification	#6206	-
Weight	16.5	kg

4.2.3 Pressure transducers

The experimental setup consist of two circumferential pressure tapings specifically to measure pressure at the turbine inlet, turbine outlet. The SENSYS pressure transducers of measurement capacity up to 300KPa were installed in the setup pipeline. Pressure transducers were used in the turbine inlet and outlet. Table 4.4 shows the standard specification of the pressure transducer.

Table 4.4 Pressure transducer spec

Model.no	PSCK0300RCPG
Pressure range	0-300kPa
Full scale output	0.052-10.003VDC
Full scale	9.951VDC
Non-Linearity	0.005 FS
Hysteresis	0.010 FS
Repeatability	0.000 FS
Accuracy	0.011 FS

4.2.4 Flow meter

The electromagnetic flow meter used in this analysis. It is a combined type flow meter basically because the flow sensor and display unit both are embedded together in a single unit. The model number of flow meter is KTM 800. The basic principle behind operation of this type of flow is the measurements of fluid flow through the flow meter which generates a magnetic field proportional to the flow velocity. The flow meter detects the change in the magnetic field the flow meter for flow measurement provides instantaneous values as well as cumulative values of the flow rate. The signal type used in the flow meter is DC 4-20mA. This type of flow meter can give highly accurate output. Flow meter specification given in Table 4.5.

Table 4.5 Flow meter specification

Connection	Standard JIS10K Flange
Size	10A (3/8")-200010A (80")
Measured flow	Water
Flow range	0.005-112926.96m ³ /h
Power	AC 1410/220V
Frequency	50-60Hz
Display	LCD Display, Flow rate:5-digit display

	Total: 9-digit Display with Backlight
Output	Analog: 4-20 mA, Pulse : DC 16-30V (open collector Pulse), Digital : RS485 (Option)
Accuracy	$\pm 0.5\%$ F.S (Option $\pm 0.2\%$) F.S)



Figure 4.6 Flow meter KTM-800

4.3 Calibration and Uncertainty Analysis

Calibration and uncertainty analysis for the sensors used for the measurements performed before the measurements were conducted. Calibration of the instruments and sensors was performed for the magnetic flow meter, torque transducer, inlet and differential pressure transducers, and miniature pressure sensors as shown in Fig 4.7.



Figure 4.7 Pressure and torque transducer Calibration sheet

As for the torque transducer, it was calibrated using a simple load and lever technique. Using known weights and marked lever, a known value of torque about the central axis was exerted on the transducer. Correspondingly, the measured input signal (voltage) on the transducer was recorded for varying moments about the central axis. The values were then used to plot voltage as a function of torque producing a linear relationship which were then used to calibrate the coefficients of the torque transducer equation to accurately measure the torque. Calibration was carried out for minimum to maximum values of torque that can be measured by the transducer.

4.4 Experimental procedure

The turbine includes a spiral casing, distributor with 6 stay vane, 13 guide vanes, a runner with 13 blades and conical type of draft tube as shown in chapter 3.

Turbine was tested by varying parameters such as guide vane angle in 6 different cases ranging between 2-12 degrees and speed of 500-1700 rpm respectively.

4.4.1 Starting the Pump

In starting the 2 pumps, the gate valve is opened as fast as possible by the time the switch of the pump is pressed to the ON position. If the pump is not properly primed, the centrifugal pump would not be able to pump water.

4.4.2 Starting the Francis turbine

After turning of the pump, water will come through the pipes and into the Francis turbine. The pumps started to generate pressure head turbine. A valve on the turbine was set to open to allow running water to enter the turbine. This valves provides and regulates the flow of cooling water for the brake shoe of the brake.

4.4.3 Hydraulic efficiency of experimental

The dimensionless speed (N_{ED}) and discharge (Q_{ED}) of the turbine expressed;

$$N_{ED} = \frac{n \times D}{\sqrt{H}} \quad (4.1)$$

$$Q_{ED} = \frac{Q}{D^2 \sqrt{E}} \quad (4.2)$$

$$E = g \times H \quad (4.3)$$

Where;

- n - Runner speed
- Q - Discharge
- E - Specific hydraulic energy

Result of the experimental data summarized in Table 4.6

Table 4.6 Experimental results of the turbine

Cases	N_{ED}	Q_{ED}	$H[m]$	$\eta[\%]$
1	63	0.194	4.16	80.0
2	65	0.19	4.16	85.8
3	76.5	0.17	6.8	74.67
4	92	0.13	7.6	88.37

Figure 4.8 and Figure 4.9 show the plot of the efficiency of the turbine obtained when operated at various speed and various guide vane angle.

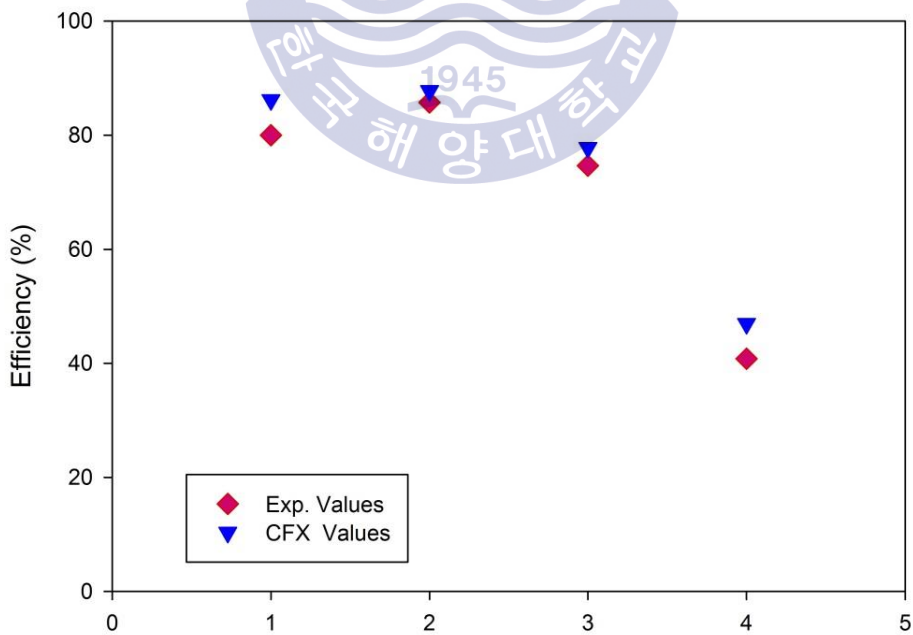


Figure 4.8 Comparison result of experimental and CFD

The lowest difference between the experimental and numerical results was 2.03% and maximum difference between the experimental and numerical results was 6.12 %. Numerical efficiency higher then experimental efficiency.

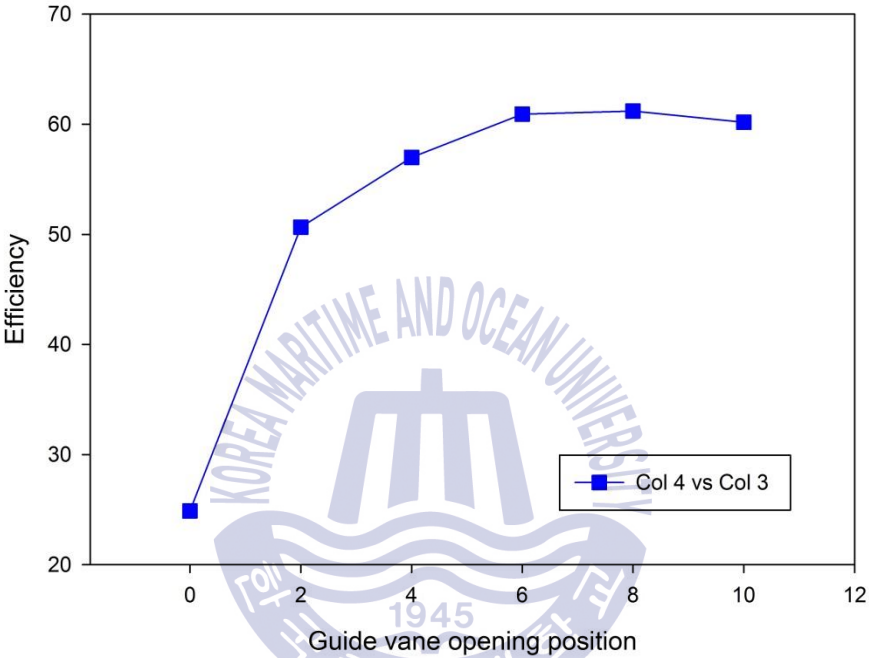


Figure 4.9 Turbine efficiency by varying guide vane angle

4.5 PIV experiment

Particle image velocimetry (PIV) is an experimental tool in fluid mechanics and aerodynamics. The basic principle involves the photographic recording of the motion of microscopic particles that follow the fluid or gas flow. Image processing methods are then used to determine the particle motion, and hence the flow velocity, from the photographic recordings. Provided there are enough particles within the area of flow under investigation, the entire velocity field of the flow can be determined. A typical PIV setup consists of a CCD camera, high power laser, an optical arrangement to convert the laser output light to a light sheet, tracer particles and the synchronizer [31].

4.5.1 Overview of PIV Flow Visualization

Understanding the flow characteristics such as the velocity and the pressure of the flowing fluid is an indispensable factor for solving all problems related to fluid engineering. Conventional flow visualization techniques provide an intuitive and easy to understand image using appropriate illumination devices, tracking particles, and a camera that can record them so that any complex flow field can be easily understood. However, quantitative flow information, for example, the provision of data such as the velocity vector value of the entire flow field that changes with time is in principle ineffective, making hydrodynamic rigorous interpretation difficult. In this context, particle image velocimetry (PIV), which combines the traditional qualitative visualization technique and digital image processing technology, has been introduced in the early 1980s as a new experimental technique for speed measurement. In recent years, computational fluid dynamics (CFD) and it is widely regarded as a representative measurement technique of the flow field which surpasses merits. The basic principles of PIV are as follows. That is, the local velocity of the flow field can be easily obtained by knowing the straight line distance and direction in which the fine tracked particles passing through a certain point move for a minute time. That is, it can be easily obtained from the relationship between the time interval and the vector displacement required for arbitrary particle motion. By distributing tracer particles with the same specific gravity as the fluid in the flow field and

interpolating the instantaneous distribution of these particles in space with two images with minute time differences (for example, cross-correlation technique). Therefore, in principle, it can be easily expanded to two-dimensional as well as three-dimensional. Recently, three-dimensional velocity field measurement methods such as Stereoscopic PIV and Volume PIV have been developed and widely used in fluid analysis studies. Therefore, the PIV technique can fundamentally solve the limitations of the point measurement of LDV and the like, and it is able to solve the limitation of the point measurement of LDV, and it is possible to develop a high-performance PC, high-resolution CCD camera, image input devices such as high-speed camera and reliable data processing software, We maintain our position. Currently, a time-resolved PIV known as dynamic PIV is widely used. In this case, high resolution (1K x 1K) and high-speed camera (500-2000 fps at full frame) are used. In Dynamic PIV, it is necessary to support proprietary software that can easily create basic information such as velocity vector distribution as well as animation of flow information as a post-processing technique.

4.5.2 Configuration of PIV experiment device

Figure 4.10 shows a device of the PIV experiment. It is made of transparent acrylic which is suitable for visualizing the flow field inside PTO experiment device. The camera mount is made so that camera can be fixed according to a position because we have to measure with a high speed camera on ocean simulator where motion occurs. Figure 4.11 shows the 3D view of the draft tube.

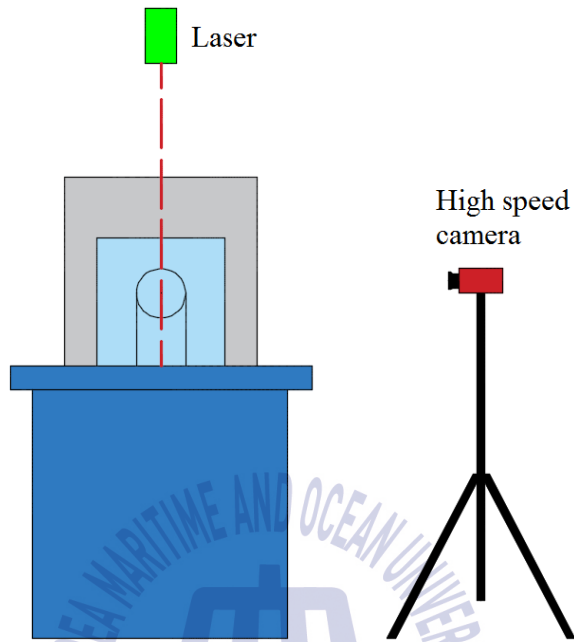


Figure 4.10 PIV experimental setup

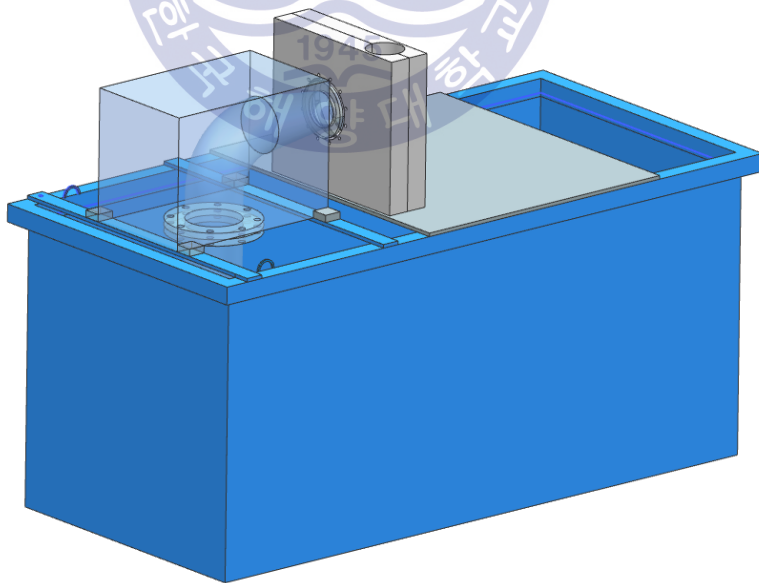


Figure 4.11 3D view of the acrylic draft tube

4.5.3 Lighting and tracking particles

In order to perform image processing, it is absolutely necessary to supply appropriate illumination to the measurement cross section to be measured. This illumination contributes to acquiring clear and contrast - free images by making the surface scattered light image of the tracer particles injected into the flow field have higher gray level than the surrounding background image. Particularly, in order to obtain a clean image in a high-speed flow field, a high-power light source is generally required. In this experiment, a maximum of 4W DPSS laser is used and green light is generated. The light emitted from the laser is usually a circular straight light with a diameter of 2 mm and a 2-dimensional sheet light with a thickness of about 2 mm is made through a cylindrical lens.

PIV is a method to obtain velocity vector data by computer analysis of particle images that are uniformly distributed in the flow field during a short period of time. Therefore, selection of particles to be used has a great influence on measurement accuracy. Generally, the tracer particles must be good in scattering at the surface and small in density of the particles and the working fluid, so that traceability should be excellent. The smaller the diameter of the particle to follow the flow of the fluid, the larger the particle size should be to some extent to enable the camera to acquire the particle image by scattering. In normal air, the size is usually in the range of several micrometers to several tens of micrometers. In liquids such as water, particles of several tens of to several hundreds of are used because the size is not restricted. In this study, spherical PVC particles with an average specific gravity of 1.02 and an average diameter of 100 μm were used as tracer particles. A digital high-speed camera (Photron Fastcam SA3) with a high resolution of 1024 (H) x 1024 (V) was used as the image input device. Since the frame rate is fixed at 30 frames / second in general CCD camera or home camcorder, it is difficult to measure speed more than 0.5m / sec in such input equipment and it is difficult to take continuous photograph which can secure the unsteady characteristic of the flow field. The problem of time-series flow phenomena is problematic. To solve this problem, a high-speed camera is widely used. Using a camera of about 1000 fps, it is possible to continuously store a flow field of about 10 m / s. It is suitable for dynamic PIV application and animation production because it

can take a lot of continuous images at high speed. It can record up to 7,500 frames per second with a segment resolution of 256x256 pixels. This image is inadequate for general flow field analysis because only a small part of the flow field can be measured. This camera is 1000 fps in full frame.

Figure 4.12 shows the acrylic draft tube before starting the experiment.

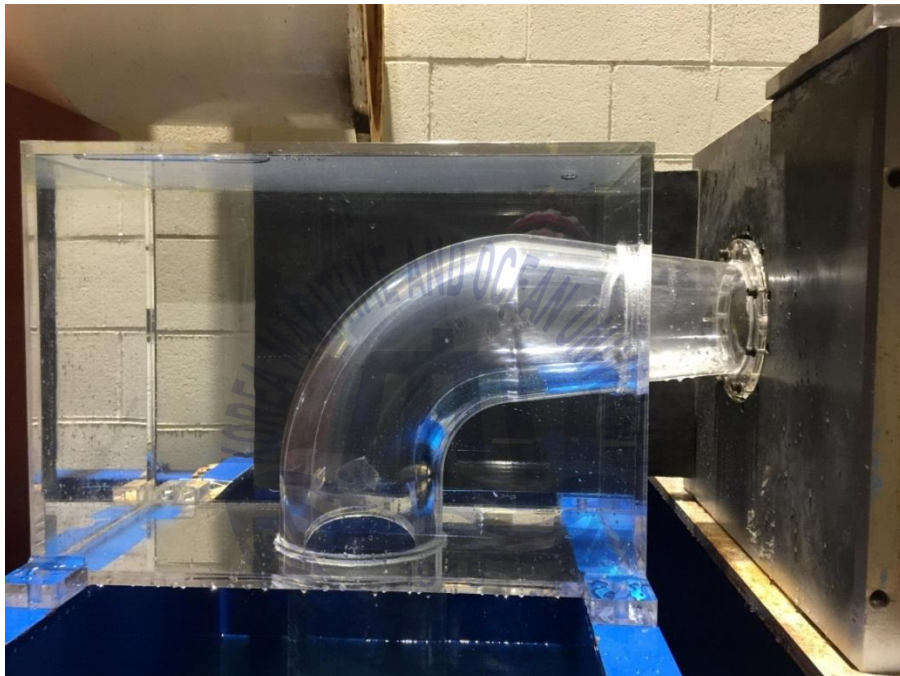


Figure 4.12 Acrylic draft tube

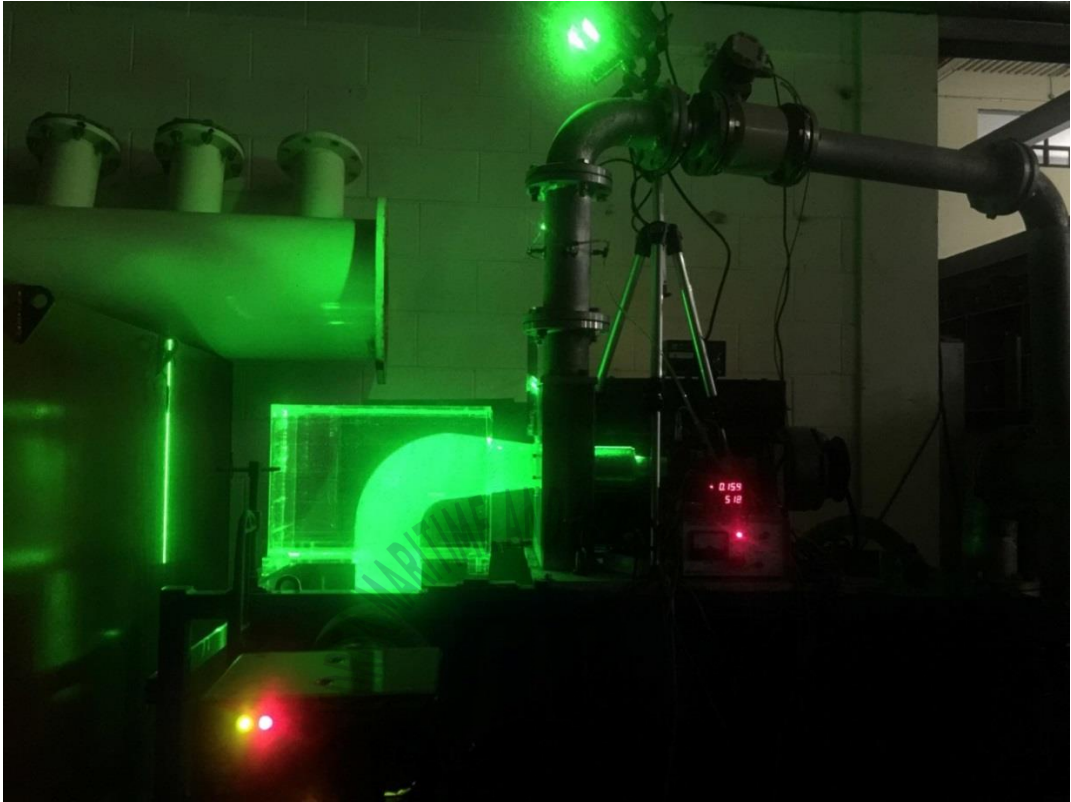


Figure 4.13 PIV experimental arrangement



4.5.4 Result of the PIV experiment

Using PIV measurement, flow pattern and characteristics was studied and hereby discussed.

Figure 4.13 shows the procedure of the experimental on operating condition with 1300 rpm.

Figure 4.14 shows cavitation phenomenon that occurs. However, it is important noting that these occurs outside the operating condition. At much higher rotational speeds, bubbles form at the draft tube inlet and flows downstream. The flow is violent as observed in the figure. Chaotic flow is unwanted and must always be avoided. Given that cavitation occurs outside the specified operating range of the turbine, the system is operating within safe zones and will less likely to be subjected to violent vibrations that can lead to mechanical failure.

Figure 4.15 shows axial velocity vectors inside mid-section of the draft tube. Noticeably, velocity vectors at the wall boundaries is missing mostly because in these wall sections, the flow was mostly tangential i.e. it circulated around the central axis of the tube along the walls. This behavior was consistent along the length of the draft tube. This circulation is due to the rotation of the turbine which imparted its rotational behavior onto the fluid near the walls which then entered the draft tube with a high tangential velocity component. Therefore the flow near the walls of the draft tube circulates around the central axis as it moves down the draft tube. This is the reason why velocity vectors near the wall cannot be seen as only axial velocity components can be recorded in the 2 dimensional view.

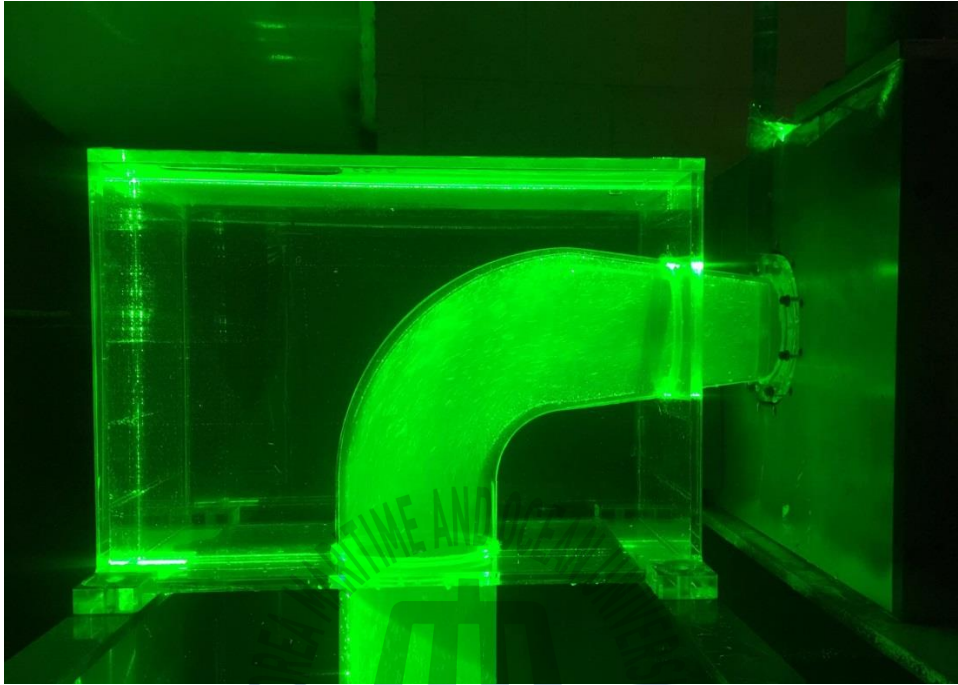


Figure 4.14 Flow pattern at operating condition

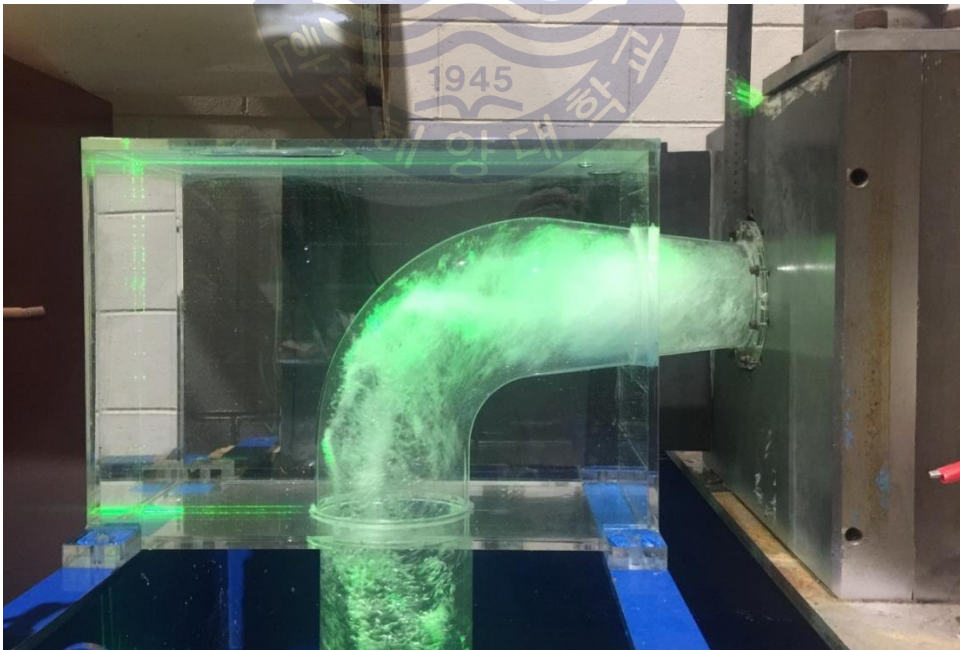


Figure 4.15 Flow pattern at cavitation condition

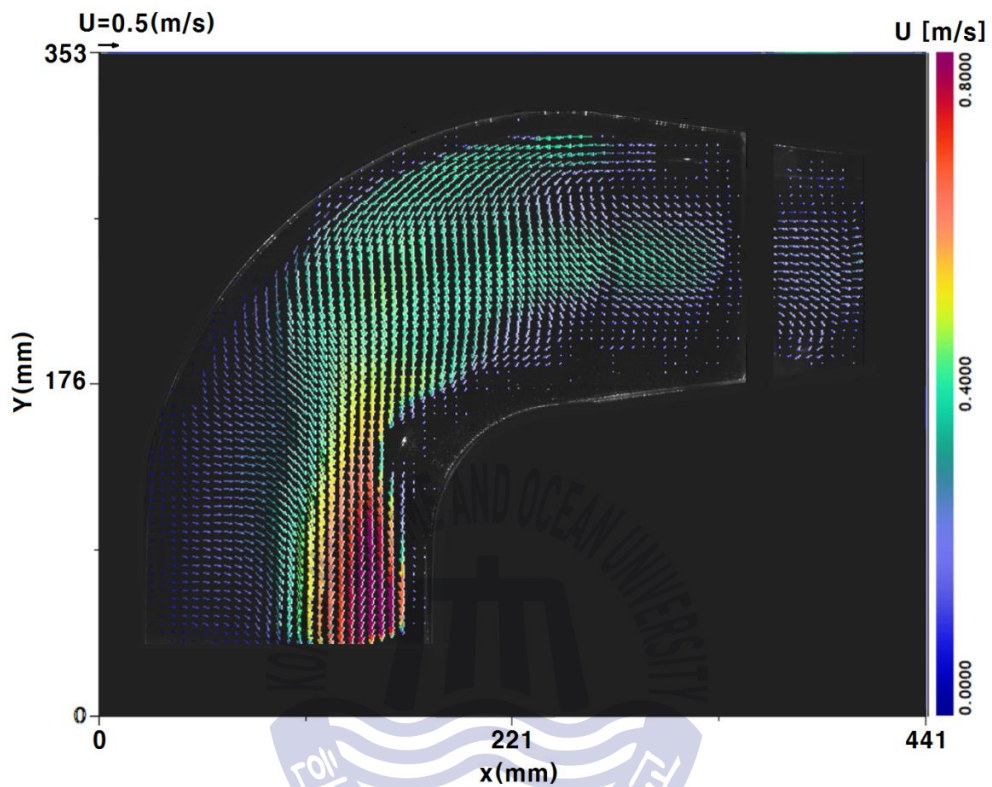


Figure 4.15 Average velocity vector

Furthermore, flow next to the central axis as it comes through the inlet flows back on itself. It does so until it encounters the incoming tangential flow from the walls of the tube and joins it. It then becomes part of the circulating flow on the outside walls which have high tangential velocity components and therefore cannot be seen in Fig 4.15. Flow in between the central axis and the walls have low tangential velocity component and higher axial velocity component. The circulation for this flow region is much less than that on the outside walls. However, it is still circulating. The absolute velocity is maximum for flow on the outside walls in comparison to that near the central axis.

Figure 4.16 shows a 3 dimensional perspective on flow behavior inside the draft tube. The streamlines show the distinct flow pattern on the respective regions. The blue streamline

clearly shows that flow on the outside walls are circulating around the central axis of the tube as it flows along the tube. Correspondingly, flow velocity is maximum for these region of the tube. This also proves that the tangential velocity component is higher than the axial component. The red streamline shows that flow near the central axis reverses. It turns back and joins the strong circulating flow near the walls which then proceeds forward. The purple streamline represents flow in between the central axis and the draft tube walls. These flow is still circulating but the axial velocity component is greater. Overall, the circulating flow for the different regions of the turbine results in vortex downstream of the draft tube. The circulating flow is mostly due to the arrangement and rotation of the turbine. Overall, maximum flow velocity occurs near the walls of the draft tube.

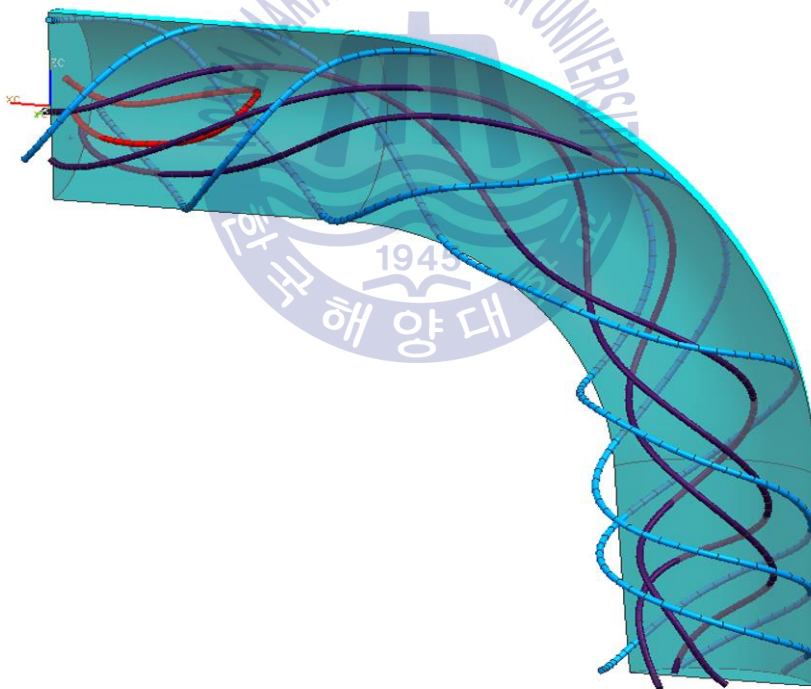


Figure 4.16 3D Streamline pattern

Figure 4.17 shows the horizontal and vertical axial velocity vectors. For flow near the central axis, the horizontal velocity vectors are directed backwards toward the inlet. Near the inlet of the tube the magnitude of the velocity vectors are greater. This shows that backflow occurs for this region of the tube in which the tendency for backflow is greater near the draft tube inlet. In between the central axis and the walls, tendency for backflow is less and the fluid mostly has a positive horizontal velocity component which results in forward flow. Near the walls, the velocity vectors cannot be measured as flow is largely tangential in this region. Along the bend and the vertical section of the draft tube, vertical axial velocity component dominates for flow around the central axis of the draft tube. Maximum velocity was recorded for vertical axial velocity component. For flow between the central axis and the right wall of the tube, the velocity component is mostly dominated by the horizontal components which results in circulation of the flow and hence vortex formation. Figure 4.18 shows the kinetic energy in the draft tube.

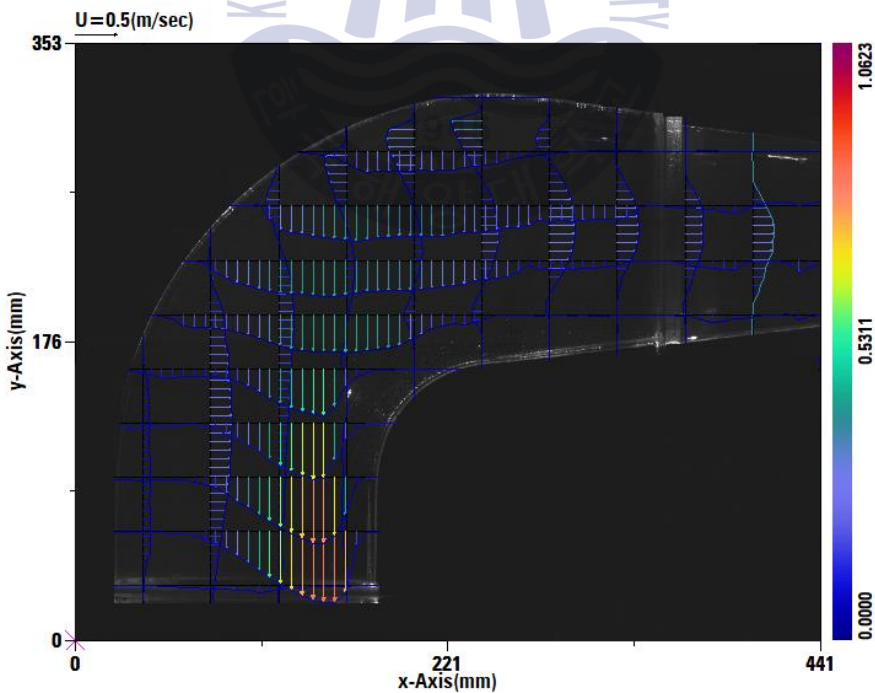


Figure 4.17 Average velocity line

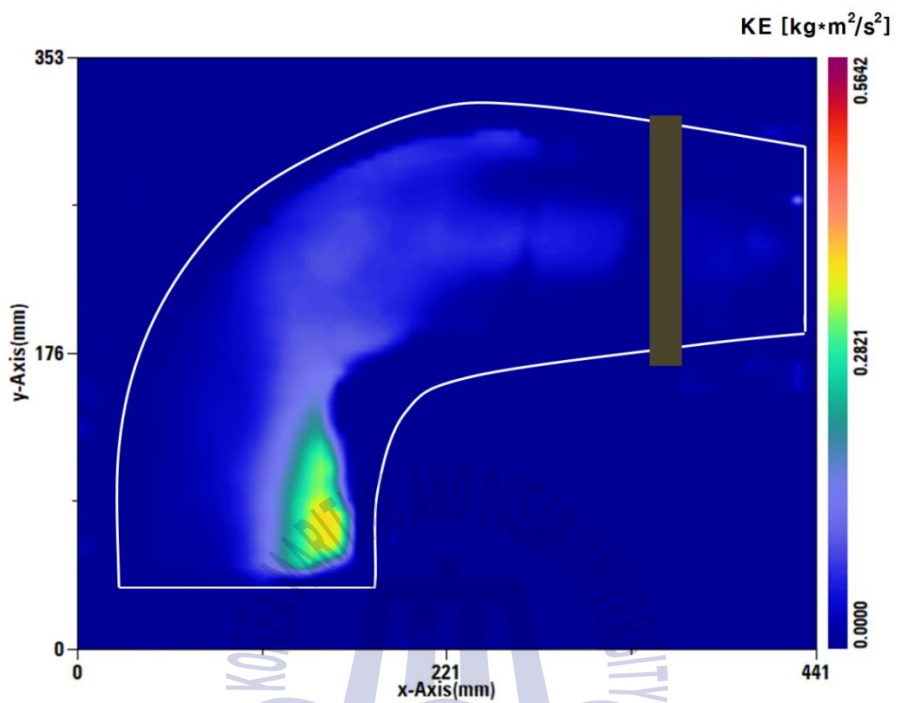


Figure 4.18 Kinetic energy in the draft tube

CHAPTER 5. CONCLUSION

In this study, a micro-class Francis hydro turbine of 3KW output was designed and its flow dynamics was numerically analyzed using CFX software. Optimization was performed on CFD that signifies reducing simulation and cost of design. Time dependent analysis figured out pull load, part load condition with misaligned guide vane. In numerical simulation, different sets of operating points were selected to get performance characteristics of the turbine and best efficiency point indicated 91.67% efficiency at 0.02m³/s, power output 3.32KW. Performance of the turbine is improving as moving towards BEP from part load due to reduction of head loss in guide vane, draft tube and runner while in case of spiral casing head loss increases. Vortex shedding is a main operational problem in Francis turbine. Several researchers have considered to reducing the vortex shedding using different control techniques. With small size turbine, the level of vortex control techniques also showed moderate effect in swirl control. For misaligned guide vanes, more options can be tried out by misaligning more guide vanes, at higher angles. Additionally, based on the numerical analysis of a Francis turbine, the results for efficiency obtained from simulation are found to good agreement with the model results obtained from manufacturer.

From the performed experiment on performance test of Francis turbine using the Francis turbine experimental set-up in the Flow Informatics Laboratory at Korean Maritime and Ocean University. The experimental analysis of the turbine showed significant result. The turbine operated at different vane angle setting were obtained. Turbine was tested varying parameters as a guide vane angle in the 6 different range of between 2-12 degrees, speed and 500-1700 rpm respectively. The lowest difference between the experimental and numerical results was 2.03% and maximum difference between the experimental and numerical results was 6.12 %. Numerical efficiency higher then experimental efficiency. Finally, experimental study was done on PIV measurement. The investigation focuses on operating condition for which flow pattern and characteristics was studied and hereby discussed

ACKNOWLEDGEMENT

This thesis becomes a reality with the kind support and help of any individual. I would like to extend my sincere thanks to all of them.

First of all, I would like to express my sincere gratitude to my supervisor Prof. Dr. Young Ho Lee for his great support, guidance and encouragement during this master's course.

I would like to offer my special thanks to my Mongolian supervisor Mr. Boldbaatar who gave me this opportunity to meet Prof. Dr. Young Ho Lee

I am deeply indebted to my supervisors in the rest of my life.

I am also grateful to the thesis committee Young-Do Choi and Dong Woo Sohn for their direction dedication and invaluable advice in this study.

I have received generous support from Dr. Chang-Goo Kim, Dr. Ji-Hoon Park, Mr. Incheol Kim, Mr. Ayham Amin Alhabashna, Mr. Batbeleg Tuvshintugs, and Mr. Chanaka Weerasena. I would like to acknowledge Mr. Byung-Ha Kim and Mr. Mesake Navunava especially for their assistance in my experimental study.

Finally, I would especially like to thank my amazing family for the love, support, and constant encouragement I have gotten over the years. In particular, I would like to thank my parents and sister.

REFERENCES

- [1] Wagner, Hermann-Josef, and Jyotirmay Mathur. Introduction to hydro energy systems: basics, technology and operation. Springer, 2013, pp. 126-210.
- [2] www.coursehero.com/file/ps3rb5/Module-5-Assignment-1-LASA-2-References-California-Energy-Commission-Retrieved/.
- [3] World energy statistics. IEA World Energy Statistics and Balances, 2016.
- [4] "Equipment and Processes." Solid Fuels Combustion and Gasification Dekker Mechanical Engineering, 2010, pp. 43–78.
- [5] Jaffee, R.i. Titanium Steam Turbine Blading, 1990, pp. 1–25.
- [6] Ebara transfers hydro turbine business to Voith Fuji Hydro. Pump Industry Analyst, Vol. 2011, No. 4, 2011, pp. 1-13
- [7] Blazek, J. "Turbulence Modelling." Computational Fluid Dynamics: Principles and Applications, 2001, pp. 225–265.
- [8] M.F. Gubin, Draft Tubes of Hydraulic Station, Amerind Publishing Company Pvt. Ltd, 1973.
- [9] Cattanei, A., et al. "Analysis of a Numerical Model for the Oscillatory Properties of a Francis Turbine Group." Hydraulic Machinery and Cavitation, 1996, pp. 681–690.
- [10] Agarwal, Tarang, et al. "Numerical and Experimental Analysis of Draft Tubes for Francis Turbine." Indian Journal of Science and Technology, Vol. 10, No. 21, Jan. 2017, pp.1–11.
- [11] Galván, Sergio, et al. "Numerical Optimization of the Inlet Velocity Profile Ingested by the Conical Draft Tube of a Hydraulic Turbine." Journal of Fluids Engineering, Vol. 137, No. 7, 2015, pp. 25-31.
- [12] Weeks, David E., and David G. Hull. "Optimum flat-Top airfoils in viscous hypersonic flow." Journal of Optimization Theory and Applications, Vol. 5, No. 1, 1970, pp. 52–66.
- [13] Kerschberger, Peter, and Arno Gehrler. "Performance Optimization of

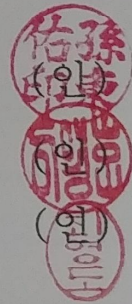
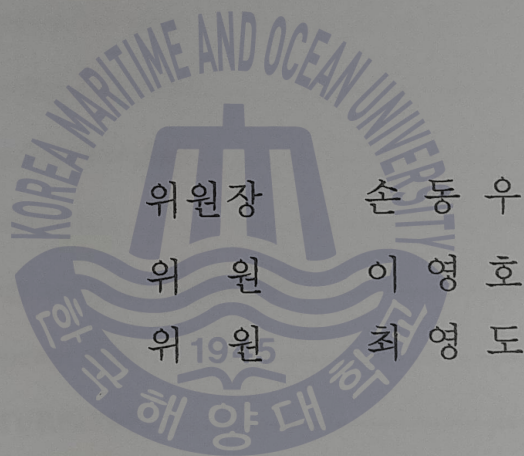
- High Specific Speed Pump-Turbines by Means of Numerical Flow Simulation (CFD) and Model Testing.” *International Journal of Fluid Machinery and Systems*, Vol. 3, No. 4, 2010, pp. 352–359.
- [14] Shi, Qinghua. “Experimental Investigation of Frequency Characteristics of Draft Tube Pressure Pulsations for Francis Turbines.” *Hydraulic Machinery and Cavitation*, 1996, pp. 935–944.
- [15] Stoessel, Lucien, and Håkan Nilsson. “Steady and unsteady numerical simulations of the flow in the Tokke Francis turbine model, at three operating conditions.” *Journal of Physics: Conference Series*, Vol. 579, 2015, p. 012011.
- [16] Liangjun Cheng. *On the Problem of Hydro-Vibration of Francis Turbines*. *Journal of Huazhong University of Science and Technology (NatureScience Edition)*, 2011, Vol 6, pp.61–66.
- [17] Gang Wu, Yongfeng Dai, Kewei Zhang, & Yuecan Tan. Relations between Flow Field and Pressure Fluctuation in Draft Tube of Francis Turbine. *International Journal Hydroelectric Energy*, 2000, Vol 18(1), pp.58–61.
- [18] Nishi, Michihiro, and Shuhong Liu. “An Outlook on the Draft-Tube-Surge Study.” *International Journal of Fluid Machinery and Systems*, Vol. 6, No. 1, 2013, pp. 33–48.
- [19] Tony Lee Wahl., *Draft tube surging hydraulic model study.*, Ph.D. Colorado: Colorado State University, 2011.
- [20] Finnemore, E. John, and Joseph B. Franzini. “Fluid mechanics with engineering applications”. McGraw-Hill, 2009.
- [21] Noye, John, and C. A. J. Fletcher. *Computational techniques and applications, CTAC-83: proceedings of the 1983 International Conference on Computational Techniques and Applications*, held at the University of Sydney, Australia. North-Holland, 1984, pp.553-64.
- [22] Li, S. C. “Introduction.” *Series on Hydraulic Machinery Cavitation of Hydraulic Machinery*, 2000, pp. 1–8.
- [23] Maki, Hiroshi, and Yasuo Mori. “On the Study of the Flow through an Impeller of Mixed and Inward-Flow Radial Turbines : 3rd Report, Interference with the Flow from the Circular Nozzle.” *Bulletin of JSME*, Vol. 16, No. 91, 1973, pp. 81–92.
- [24] Chen, Zhenmu, et al. “The effect of runner blade loading on the

- performance and internal flow of a Francis hydro turbine model.” *Journal of Mechanical Science and Technology*, Vol. 30, No. 4, 2016, pp. 1617–1623.
- [25] Wei, Q S, et al. “Application of J-Groove to the suppression of swirl flow in the draft tube of a Francis hydro turbine.” *IOP Conference Series: Earth and Environmental Science*, Vol. 15, No. 2, 2012, p. 022017
- [26] Qian, Z D, et al. “Analysis of pressure oscillations in a Francis hydraulic turbine with misaligned guide vanes.” *Proceedings of the Institution of Mechanical Engineers, Part A: Journal of Power and Energy*, Vol. 224, No. 1, Aug. 2009, pp. 139–152
- [27] Kc, Anup, et al. “CFD study on prediction of vortex shedding in draft tube of Francis turbine and vortex control techniques.” *Renewable Energy*, Vol. 86, 2016, pp. 1406–1421
- [28] Atmaram Kayastha. *Numerical and Experimental Analysis of a Hydro Cyclone Separator for Sediment Laden Micro Hydro Francis turbine*, 2015, Master’s thesis, Korean Maritime and Ocean University.
- [29] Scarano, Fulvio. “Particle Image Velocimetry.” *Encyclopedia of Aerospace Engineering*, 2010
- [30] Chirkov, D, et al. “CFD simulation of pressure and discharge surge in Francis turbine at off-Design conditions.” *IOP Conference Series: Earth and Environmental Science*, Vol. 15, No. 3, 2012, p. 032038
- [31] Duquesne, P, et al. “Flow separation in a straight draft tube, particle image velocimetry.” *IOP Conference Series: Earth and Environmental Science*, Vol. 22, No. 3, Jan. 2014, p. 032004
- [32] Jošt, Dragica, and Andrej Lipej. “Numerical Prediction of Non-Cavitating and Cavitating Vortex Rope in a Francis Turbine Draft Tube.” *Strojniški vestnik – Journal of Mechanical Engineering*, Vol. 57, No. 06, 2011, pp. 445–456.
- [33] Wang, Zhengwei, and Lingjiu Zhou. “Simulations and Measurements of Pressure Oscillations Caused by Vortex Ropes.” *Journal of Fluids Engineering*, Vol. 128, No. 4, 2006, p. 649
- [34] Sozen, Adnan, et al. “Determination of the Effect of the Angle of the Wicket Gate on Turbine Efficiency in Francis Type Turbines by CFD Analysis.” *International Journal of Fluid Mechanics Research*, Vol. 42, No. 1, 2015, pp. 1–12.
- [35] “Efficiency Analyses for Small Hydro Power Plant with Francis Turbine.” *International Journal of Modern Trends in Engineering &*

Research, Vol. 4, No. 10, Jan. 2017, pp. 155–164



본 논문을 Enkhtaivan의 공학석사 학위논문으로
인준함.



2017년 12월 27일

한국해양대학교 대학원